Constraining the contributions of Penguin diagrams to the phase shift of ϕ_s through $B \to DD$ decays

Leander van Beek
Rijksuniversiteit Groningen
l.v.van.beek@student.rug.nl
06-04-2021

Daily Supervisor
dr. K. A. M. De Bruyn
k.a.m.de.bruyn@rug.nl
Second Examiner
dr. ir. C.J.G. Onderwater
c.j.g.onderwater@rug.nl

Abstract

In this thesis, the measurement of the CKM-parameter ϕ_s from B to DD-meson decays will be analysed taking the next-to-leading order Penguin diagrams into account. This is a requirement to correctly interpret higher precision measurements of this Standard Model parameter or constrain contributions of New Physics. Sizing these corrections is done by determining the Penguin parameters from the $B_d \to D_d^+ D_d^-$ decay, which can be related to the $B_s \to D_s^+ D_s^-$ decay by U-spin symmetry. The analysis results in a correction of $\Delta\phi_s = (-0.2 \pm 0.6)°$. The measurements of $\phi_s^{eff} = (1.0 \pm 9.7)°$ are correspondingly shifted towards $\phi_s^{corr} = (1 \pm 10)°$. The shift brings the measurement closer to the Standard Model prediction, but at current precision the corrections of the Penguin parameters are still in the margin of error. An estimate is made of the implications of the reducing uncertainty while measurements are being taken.

rijksuniversiteit groningen

Contents

Chapter 1

Introduction

1.1 A General Introduction

The Standard Model of Particle Physics has been constructed over the past century as a theory that incorporates all elementary particles and three out of the four fundamental forces that are currently known. Analysing the predictions of the Standard Model, its limits, and possible extensions is still a very active field. As the Standard Model is very extensive, only a subsection of the theory is covered in this project: flavour physics. Flavour physics is the section of the standard model that considers the six flavours quarks and leptons and how these interact with each other. Specifically, the mechanics of the decay $B_q \to D_q^- D_q^+$ are investigated and compared to theoretical predictions of the Standard Model.
The Standard Model predicts coefficients that relate to the transition between different quark flavours. These coefficients can also be measured in particle detectors such as LHCb at CERN in Geneva, Switzerland, and Belle II, located at KEK in Tsukaba, Japan. These measurements are currently however not taking the complete picture into account. In this project, the interpretation of these measurements will be updated. As a complementary effect, this updated interpretation of measurements allows for the possible assessment of contributions of New Physics effects. The term New Physics is used for theories that are an extension to the Standard Model that may solve some of the problems in current formulation of the Standard Model. Because although the Standard Model gives very accurate predictions for some observations, the fact that only three out of the four fundamental forces are implemented already shows that it is not a theory of everything.
Completing this project successfully will hence result in a better understanding of the dynamics of $B_q \to D_q^- D_q^+$ decays in the Standard Model and allow for assessing any effects of New Physics to help completing the holes in the theory.

1.2 Getting slightly more technical

The goal of this research is to better constrain a parameter measured in the $B_q \to D_q^- D_q^+$ by adding a correction from the theory to get a better idea of what it is that is actually measured in experiments. To relate the experimental measurements to the parameters that describe the

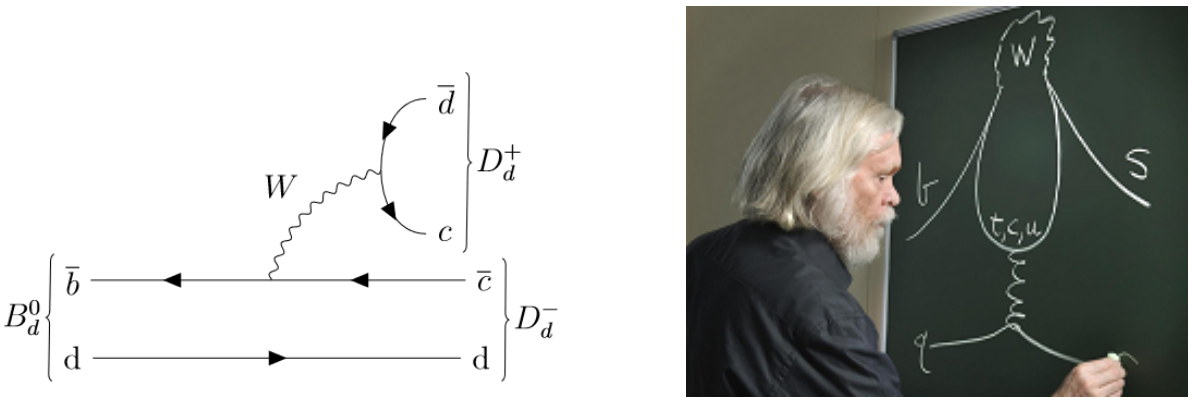

Figure 1.1: A Tree- (left) and Penguin Diagram (right).

system, an underlying theoretical foundation is required. Currently, this theoretical foundation is not applied in a futureproof manner.
The flavour transitions between quarks are encoded in the Standard Model through the so-called CKM-matrix. This matrix contains elements that represent the strength of a transition probability between the three quark generations. The elements of the CKM-matrix can be determined by observing decays from known particles and determining the decay products. The theory for these transitions of the weak force were first developed by Cabibbo in the Cabibbo matrix [1], which interconnected the first two generations of quarks. This model was extended to the Cabibbo-Kobayashi-Maskawa (CKM)-Matrix halfway through the 70s [2]. By doing this, Kobayashi and Maskawa naturally implemented a similar connection to a hypothesized third generation of quarks. In 1977 the first quark from this generation was discovered; the bottom quark. For this work, Kobayashi and Maskawa were awarded the Nobel prize in 2008 [3]. It is interesting that Cabibbo, who laid the foundation of the model initially all by himself, was not awarded a part of this prize. The Nobel committee's explanation was that they did not include Nicolo Cabibbo because they mainly awarded the prize for discovering the existence of the third generation of particles - some say an idea that Cabibbo was initially not supportive of.

Measuring parameters from the Standard Model directly is often not possible and results in the need to combine measurements that depend on the same set of parameters. In this research, it is actually required to combine measurements from two different decay channels: $B_s \to D_s^+ D_s^-$ and $B_d \to D_d^+ D_d^-$. One might ask the justified question of whether this is actually a valid approach. A well-known approach for determining the dependence of a system on a parameter is keeping everything else constant and only varying the parameter of interest. As this approach is not viable in this situation, refuge is sought in symmetry arguments that are built into the Standard Model.
Because nature seems to adhere to certain symmetries, these symmetries are also built into the Standard Model. In this research, the argument is made that because of U-spin symmetry, decays that are related by the interchange of all $d \leftrightarrow s$ are similar enough that conclusions can be drawn on the U-spin partner of one decay. This is exactly what makes up the difference between the $B_d \to D_d^+ D_d^-$ and $B_s \to D_s^+ D_s^-$ decays, such that 'invoking' this symmetry allows for the relation of the decays.

It is interesting to note that not only will symmetries in the Standard Model allow the strategy employed to find the desired parameters, but also that the violation of a symmetry is what results in our observables. Sometimes these symmetries turn out not to be there, or they only hold in certain limits. This symmetry is the CP-symmetry, which is the combined operation of changing the sign of all spacial coordinates (P) and negating the particles' charges (C). Together, these symmetries change a particle into its antiparticle. One might intuitively think this symmetry would be a conserved quantity, but Cronin and Fitch discovered that this is not the case in the decay of the Kaon particle into two pions in 1964 [4]. The violation of this symmetry gives us a clue towards the baryon-antibaryon problem (why does the universe only exist of 'normal' matter, and is there almost no antimatter?), but it does not explain why this symmetry is broken. Even though at the time only the up, down and strange quark were observed, this experiment showed that in the parametrisation of quark transitions, CP-violation would not be possible with only two quark generations if parametrised according to Cabibbo's original theory.

The main parameter that is under investigation in this project is the parameter ϕ_s. This parameter determines the strength of the CP-violation in the $B_s^0 - \overline{B_s^0}$-meson system. The B_s^0-meson is able to transition into the $\overline{B_s^0}$ and vice versa, but this has an effect on the CP-violation in that system. Through observing this violation, it is hence possible to determine (corrections to) ϕ_s.

To better understand what these non-leading order corrections are, it is useful to understand how these decays or transitions are built up. All transitions in Particle Physics can happen in more than one way. As long as the initial- and final state are the same, it is said that all these processes contribute to the same decay. For the decays considered, that means an initial $B_{(d/s)}^0$ and eventually two $D_{d/s}^{\pm}$ mesons. Using Feynman diagrams, it is possible to draw all these diagrams to tell them apart. Not all contributions are equal, though - some of these diagrams contribute more to the decay rate than others. The Tree diagram, after its tree-like structure, shown in Figure 1.1 is the dominant diagram for the decays that will be studied here. Measurements for the parameter that is under investigation are currently only considered as a product of these Tree diagrams. In fact, there are also other diagrams at play; among others diagrams called Penguin diagrams. These carry their respective name due to an imaginative physicist being able to visualise them as the corresponding birds [5], see Figure 1.1. Their relative contributions would not make any changes to value of ϕ_s at the precision currently worked at. The process of incorporating these processes into the interpretation of our observation is the main topic of this paper.

The main topic is the phase shift that the Penguin diagrams bring to the weak angle ϕ_s. This phase shift will be denoted as $\Delta\phi_s$. Because there are still hadronic effects involved in computing the amplitude of the penguin diagrams that are not perturbatively calculable, some assumptions while comparing the decays of for example the $B_d \to D_d^+ D_d^-$ and $B_s \to D_s^+ D_s^-$ decay will be made. An important assumption is the invariance of the strong force under exchange of there $\{u, d, s\}$ quarks. Although this symmetry is not exact, the corrections are assumed to be negligible here. By making this assumption, it is possible to determine the "Penguin parameters" a and θ, which resemble the relative contribution of the Penguin diagrams

to the Tree diagram. From these Penguin parameters then follows the phase shift $\Delta\phi_s$. Using this phase shift, the experimental measurements of ϕ_s can be corrected to be more accurate. This corrected value, ϕ_s^{corr}, can then be compared to the Standard Model value. How these parameters relate to each other is most easily seen in the following equation.

$$\phi_s^{eff} = \phi_s^{corr} + \Delta\phi_s^{Pen} \tag{1.1}$$

Besides this, a short projection of possible future results we be performed. It is known that the LHCb-detector will get a significant upgrade [6] in both its precision and data collection rate. Belle II has only started collecting new data after its upgrade in 2019 [7] and will keep collecting data to improve the precision of its measurements at the current time. Based on that, we can make an estimate of what that would mean for the precision of future measurement results, and from that, the precision on the correction to the weak angles.
The data analysis will be done making use of the GammaCombo framework [**?**], which is an extension to the ROOT fitting program developed by CERN. In GammaCombo, it is possible to create modules that connect measurements and the underlying theory. Through combining these modules, the best fit parameters can be determined by Gaussian convolution of the measurements.

As often in the field of physics, the analysis done here does not stand on itself. The parameter ϕ_s is measured in multiple decay channels, among which is the $B_s \to J/\psi\phi$ decay channel [8]. Here, they also try to determine the corrections to the measurements of ϕ_s due to the Penguin diagrams, but it is possible to go even a step further. Because the precision of those results is better, it is even possible to constrain the shift due to possible New Physics in the measurements of ϕ_s. If the Penguin diagrams are taken into account and the measurements are still not lining up with the theoretical value from the Standard Model, one can start to look for other effects that cause more of a shift in the measurements. By looking at the required shift to end up at the theoretical value, an upper boundary for the phase shift due to New Physics can be set [9]. The conclusions from this research are at significantly higher precision than the results that will be obtained for the $B_s \to D_s^+ D_s^-$ decay. Looking at the difference of the uncertainty with which ϕ_s is measured for the $B_s \to J/\psi\phi$ and $B_s \to D_s^+ D_s^-$ ($\pm 1.6°$ vs. $9.7°$), it is unreasonable to expect equally precise results. Even if the shift can be determined with arbitrarily high precision, the measurement of ϕ_s itself is already reconcilable with the value computed from the Standard Model. Determining the contributions from New Physics is therefore also something that will not be attempted here. This does not mean that this research can in advance be rendered useless, though: it is always important to have a check of the used methodology. The strategy that was employed in that research is also used here. In the case that the results here are very different, for example by pushing the measurement of ϕ_s further away from the Standard Model value, the methodology should be once more closely inspected. In the discussion of this thesis these results will therefore also be compared.

Chapter 2

Theory

The research being done in this thesis lies in the flavour physics section of the Standard Model of Particle Physics - henceforth simply the Standard Model. The Standard Model is the name for the most general theory describing all known interactions in particle physics. To be able to properly understand and appreciate the topic of study, it is required to study and develop the mathematical machinery that describes this theory first. In this section, these tools will first be developed from a theoretical view. Later, a phenomenological approach will be taken as well to complete the picture and internalize the conclusions from the theory.

2.1 The Standard Model

The Standard Model of Particle Physics [10] describes the interaction of elementary particles. The Standard Model is often given in terms of a Lagrangian and often only the relevant part of the Lagrangian is discussed, as the complete theory is very extensive and still undergoing further expansion. The elementary particles in the Standard Model can be conveniently displayed in a picture, such as one in Figure 2.1. In this model the elementary particles are ordered by their intrinsic spin; all force-carrying particles are bosons (which have integer spin) and all matter particles are fermions (which have half-integer spin).

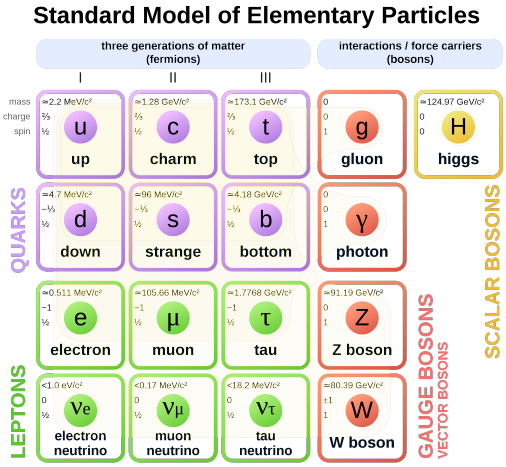

Figure 2.1: A family picture of all the elementary particles in the Standard Model.

The force-carrying particles appear as the mediators of all forces that are represented in the Standard Model; the strong force is mediated by the gluon (g), the electromagnetic force is mediated by the photons (γ), the weak force by the W and Z bosons, and mass is given to the elementary particles by interaction with the Higgs particle (H). The attentive reader might notice that the gravitational interaction is not named here. This is not a mistake - despite the combined efforts of the entire physics community, a

comprehensive theory combining gravity with the Standard Model that is verifiable by observations has not yet been formed.

The Standard Model is a quantum field theory that is built up around gauge symmetries [11]. A low-level explanation of this statement is that this theory poses that particles are no longer localised but rather extended objects through spacetime that are called fields. There are gauge symmetries imposed on these fields, which results in the gauge bosons, that mediate the interactions between the fields.

The matter particles consist of three different generations; each column makes up another generation. The second and third column of matter particles are essentially identical particles to the first column. They are identical in all properties such as charge, spin, their interaction through the strong force - only their mass is different. The masses of the fermions in each subsequent generation are strictly larger than those in the former generation. All stable matter is composed of combinations of fermions from the first generation; you can compose protons- and neutrons from up- and down quarks, use those to compose nuclei, fill their respective electron shells with electrons and voila; the foundation for building blocks of all matter has been established. All matter particles have anti-matter particles as well. These particles have the same properties as the matter particles, only their charge, additive and multiplicative quantum numbers[1] are inverted. Where matter-quarks are denoted by the first letter of their name, antimatter-quarks are denoted by the first letter of their name with horizontal line above them.

$$\text{quarks: } \begin{pmatrix} u \\ d \end{pmatrix}, \begin{pmatrix} c \\ s \end{pmatrix}, \begin{pmatrix} t \\ b \end{pmatrix}, \qquad \text{antiquarks: } \begin{pmatrix} \overline{u} \\ \overline{d} \end{pmatrix}, \begin{pmatrix} \overline{c} \\ \overline{s} \end{pmatrix}, \begin{pmatrix} \overline{t} \\ \overline{b} \end{pmatrix} \tag{2.1}$$

These building blocks of matter cannot be thrown together in any shape or form and expect to work together. You have to adhere to very strict rules to have combinations of these particles function together as a whole; these rules are described by the Standard Model Lagrangian. The interactions of these particles are often represented in Feynman diagrams. These diagrams are not only a nice graphical representation of the interactions that can take place, but they are also a useful computational tool. The rules of the calculation can be derived from the Lagrangian that describes the relevant interactions [12].

The same is true for the theory in this thesis. The complete Standard Model description is very expansive, and for the intended purposes here only a subsection has to be considered. The process of splitting up this theory is perhaps simpler than it looks; all terms in the Lagrangian of the Standard Model are products of fermions, gauge bosons, and interaction terms. By leaving out the products including interaction terms for forces that are not applicable to the problem at hand, unnecessary expressions are left out of the description of the system. Expressions that describe how two electrons interact with each other through a photon for example need not be taken into account, as only the interactions of quarks through the strong- and weak force is considered.

This is not the only way of reducing the theory. Another example can be given by considering

[1] Additive and multiplicative quantum numbers are quantum numbers of which respectively the sum and the product is conserved during a process.

Meson	Constituents	Charge Q
B^0	$d\bar{b}$	0
B^+	$u\bar{b}$	+1
B_s0	$s\bar{b}$	0
D^0	$c\bar{u}$	0
D^+	$c\bar{d}$	+1
D_s^+	$c\bar{s}$	+1

Table 2.1: Properties and quark contents of relevant mesons

the applicable symmetries to the theory under consideration. The complete Standard Model has a symmetry group consisting of $SU(3)_{color} \times SU(2)_{isospin} \times U(1)_{hypercharge}$. All the terms in the product of this symmetry have a connection with the fundamental forces in the Standard Model. This complete symmetry group only holds at extremely high energies - think energies that are hypothesized immediately after the big bang - and for processes at lower energy scales only subgroups of the Standard Model symmetries have to be considered.
An important note in the aspect of this thesis has to be made specifically on one of the symmetries of the strong force: the $SU(3)_{flavour}$-symmetry. Without going deeper into the mathematics of the Lie groups behind them, for which there exist excellent sources [13], it is stated that this has an important physical consequence. The strong interaction does not differentiate between the flavours of the quarks while interacting. The strong force is 'flavour-blind'. The symmetry is useful because the strong force will not see any difference between the flavours of the quarks. If a process that is difficult to observe is under consideration, it can be inspected indirectly by considering the process of one of its symmetry partners. An example of this is the $B_d(\bar{b}d)$ and $B_s(\bar{b}s)$ meson. As the strong interaction will not act differently on the spectator quark in the considered decays of these mesons, it is possible to draw conclusions on the dynamics of the latter based on observations of the prior, only having to keep in mind the changing dynamics from the electroweak force. The exchange of d and s quarks is considered in the proper subgroup of U-symmetry, the exchange of s and u quarks in V-symmetry and the exchange of u and d quarks in the Isospin subgroup.
Now that all elementary particles and interactions are given, it is possible to start constructing combined states. Particles that are composed of two or more quarks are called hadrons. Particles that occur in nature always have a net zero color charge, which is often referred to as being a 'white' or 'colorless' particle. Because of this constraint, the particles can appear in pairs with a color- and anti-color charge, three different color-charges, or a combination of the previous two. The particles are kept 'inside' the protons by the gluons. In this thesis, mainly the $B_{s/d}$ and $D^{0/+/-}$-mesons will be discussed, of which properties have been tabulated in Table 2.1.

Now that we have the building blocks of the Standard Model, it is possible to add in the last ingredient to the theory: interactions. Interactions can take a wide array of shapes and forms in the Standard Model. To determine how a process occurs between the initial- and final particles, the different ways of interactions all need to be considered. The most basic tool of

investigating these processes are the Feynman diagrams, which are discussed in the next section.

2.2 Feynman Diagrams, Amplitudes and Computational Tools

As mentioned in the previous section, Feynman diagrams are diagrammatic representations of interactions between particles in the Standard Model. A simple representation of a Feynman diagram is composed of external lines, internal lines and vertices. An example of such a diagram is given in Figure 2.2 for the Compton scattering process.

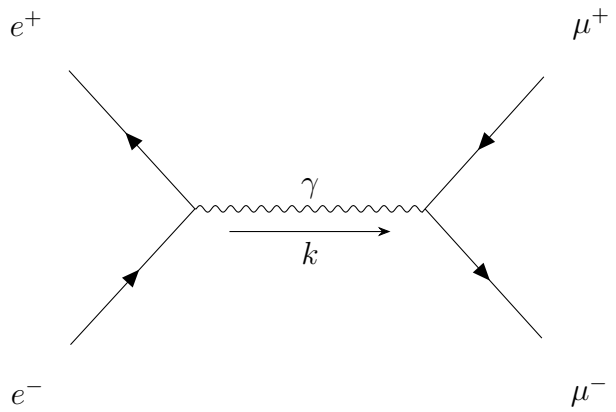

Figure 2.2: Feynman diagram for the Compton scattering process in quantum electrodynamics.

More complex diagrams can contain more complex structures inside. There exist rules for all these different components of a Feynman diagram, dependent on what section of the Standard Model is under consideration. With all these rules, the amplitude for these diagrams can be computed. The probability for a transition from initial- to final particles is the square of the sum of all these probabilities.
The amplitudes are more often than not very complicated expressions that are dependent on the momenta, spins, masses, coupling constants, and more.

2.3 CP-violation in the Standard Model

The observables that are measured in the sources for the data used in this thesis are mostly based on the manifestation of CP-violation. CP-violation is actually the violation of a conjunction of two symmetries; the parity symmetry, corresponding to the parity inversion operator P, and the charge symmetry, corresponding to the charge negation operator C [11]. The parity inversion operator inverts the spatial component of a frame of reference, i.e. $P\,|\psi(t,x,y,z)\rangle = |\psi(t,-x,-y,-z)\rangle$. The charge conjugation operator changes the sign of the charge of a particle. Although it might feel natural to assume that the P-symmetry on itself is maintained in nature

- why would particles act differently if all directions are inverted - it was shown by experiments in the fifties [14] that this was in fact not the case. To save this symmetry, it was proposed that the combination of the charge conjugation and parity inversion operators together were a symmetry of nature: the so-called CP-symmetry. A few years later however Cronin and Fitch observed CP-violation in the decay of neutral K^0-systems [4].
To understand how the discovery of CP-violation was made, it is required to understand the concept of neutral meson oscillations. As this phenomenon also plays a role in the B-mesons that are the parent particles in the considered decays, it is instructive to go over the theory of these oscillations. This will therefore be covered in the next section.
Without going too deep into the mathematics here - that will be the topic of the next section - a conceptual explanation is given here. There are a few conditions that a particle must fulfil, would it be possible for it to oscillate to its antiparticle partner. These conditions are based on conserved quantities; an electron cannot simply change into a positron because of charge conservation. A particle that is eligible to oscillate hence has to be electrically neutral. The zeroness of quantum number is not a general constraint; particles with nonzero quantum numbers such as strangeness can still oscillate into their antipartner - given that the interaction through which they do does not conserve strangeness. This last remark is an important one; since the weak interaction does not conserve the quantum number of strangeness, the neutral Kaon ($K = \{d\bar{s}\}$) is allowed to transition via the weak interaction into the anti-Kaon ($\overline{K} = \{\bar{d}s\}$).

The oscillation of the neutral mesons link to the CP-symmetry because of the following phenomenon. The eigenstates of the Kaon on which the weak- and strong force interact, are not the same. To construct a weak eigenstate of the Kaon, a superposition of the strong eigenstates can be considered. One of the superpositions is the sum of the Kaons with opposite strangeness, where the other superposition is the difference. The parametrisation then looks as given in 2.2. The subscripts S and L stand for short- and long lived respectively, as they have lifetimes that differ by three orders of magnitude.

$$\left|K_S^0\right\rangle = \frac{1}{\sqrt{(2)}}\left(d\bar{s} - s\bar{d}\right), \left|K_L^0\right\rangle = \frac{1}{\sqrt{(2)}}\left(d\bar{s} + s\bar{d}\right) \tag{2.2}$$

These K_S^0 and K_L^0 states are weak eigenstates. Both have different CP-eigenvalues; K_L^0 has $CP = -1$, while K_S^0 has $CP = +1$. It is possible to obtain a pure beam of K_L^0-mesons, because its lifetime is so much larger than that of the K_S^0-meson. From this K_L^0 meson, a decay into two Pions was found. As the CP-eigenvalue of that state is $+1$. This observation implied CP-violation. For this discovery, Cronin and Fitch received the Nobel Prize in Physics in 1980. The reason for the few in a thousand $K_L^0 \to 2\pi$ decays are no longer a mystery. It turned out that there is a small CP-impurity in the weak eigenstates K_L^0 and K_S^0. The presumed pure K_L^0 state appeared to have a small admixture of the K_S^0-state and vice versa. The coefficient of one the opposing CP-eigenstate in the wave function for the state is a measure for the CP-violation. To conclude this section: The basis for the weak- and CP-eigenstates almost perfectly overlap, but the small misalignment provides the possibility for the weak eigenstates to be projected in a final eigenstate with a different CP-eigenvalue.

There is more than one way for CP-violation to take place. There occurs violation in mixing, which happens in cases as described up to here. When the weak eigenstates do not exactly coincide with the CP-eigenstates, CP-violation in mixing occurs. The second type is direct CP-violation. It can occur when for a meson M and a decay product f, the amplitudes $\mathscr{A}(M \to f) \neq \mathscr{A}(\overline{M} \to \overline{f})$. Finally, it is possible to have violation in the interference between decays with and without mixing, with oscillations. This case occurs when for a meson M and decay product f, where $f = \overline{f}$, the decay amplitudes $\mathscr{A}(M \to f) \neq \mathscr{A}(\overline{M} \to f)$.

2.4 Neutral Meson Mixing

As was mentioned in the previous chapter, neutral mesons can oscillate into their antimatter-partners (CP-partners) and back. This is possible because the eigenstates for the weak-, strong- and electromagnetic interaction are not simultaneously diagonalizable. If the strong eigenstates of the mesons are considered, where they have definite quark contents, the oscillations between their states can be derived by making use of quantum mechanical arguments. This does not only happen for the K^0-meson in the previous section, but it also occurs for the B_d^0, B_s^0 [15], and D^0 mesons [16].
The initial step is to write down Schrödinger's Equation, describe the wave function that is considered, and note the relevant Hamiltonian.

$$i\frac{\partial \psi}{\partial t} = H\psi \tag{2.3}$$

$$\psi(t) = \begin{pmatrix} p(t) \\ q(t) \end{pmatrix} \tag{2.4}$$

$$H = H_{strong} + H_{electromagnetic} + H_{weak} \tag{2.5}$$

A simplified Hamiltonian that only describes the dynamics of meson oscillation can be written in the form of two matrices; the mass matrix M and the decay matrix Γ. These are both hermitian matrices, which constrain their elements. H itself is not hermitian.

$$H = M - \frac{i}{2}\Gamma = \begin{bmatrix} M - \frac{i}{2}\Gamma & M_{12} - \frac{i}{2}\Gamma_{12} \\ M_{12}^* - \frac{i}{2}\Gamma_{12}^* & M - \frac{i}{2}\Gamma \end{bmatrix} \tag{2.6}$$

There is an underlying assumption of CPT-symmetry here to be able to assume that the particle- and antiparticle masses are equal, but so far there is no compelling evidence to discredit that assumption. Inserting this Hamiltonian into the wave equation, the following is obtained.

$$i\frac{d\psi}{dt} = \begin{bmatrix} M - \frac{i}{2}\Gamma & M_{12} - \frac{i}{2}\Gamma_{12} \\ M_{12}^* - \frac{i}{2}\Gamma_{12}^* & M - \frac{i}{2}\Gamma \end{bmatrix} \psi \tag{2.7}$$

It is now possible to solve the eigenvalue equation to find the eigenvectors. These eigenvectors can then be related to the time dependent functions $p(t)$ and $q(t)$. These were found to be

$$\lambda_\pm = M - \frac{i}{2}\Gamma \pm \sqrt{\left(M_{12} - \frac{i}{2}\Gamma_{12}\right)\left(M_{12}^* - \frac{i}{2}\Gamma_{12}^*\right)} \tag{2.8}$$

Given that the eigenvalue equations gives the eigenvalues in the diagonal entries of a 2×2 matrix, it is possible to rephrase this to

$$\begin{bmatrix} m_1 + \frac{i}{2}\Gamma_1 & 0 \\ 0 & m_2 + \frac{i}{2}\Gamma_2 \end{bmatrix} = \begin{bmatrix} M - \frac{i}{2}\Gamma + \sqrt{\cdots} & 0 \\ 0 & M - \frac{i}{2}\Gamma - \sqrt{\cdots} \end{bmatrix} = \Lambda \tag{2.9}$$

where the diagonal eigenvalue matrix is called Λ. From here it is possible to note the mass- and decay width differences of these particles.

$$\begin{aligned} \Delta m &\equiv 2\,\mathrm{Re}\left(\sqrt{\left(M_{12} - \frac{i}{2}\Gamma_{12}\right)\left(M_{12}^* - \frac{i}{2}\Gamma_{12}^*\right)}\right) \\ \Delta\Gamma &\equiv 4\,\mathrm{Im}\left(\sqrt{\left(M_{12} - \frac{i}{2}\Gamma_{12}\right)\left(M_{12}^* - \frac{i}{2}\Gamma_{12}^*\right)}\right) \end{aligned} \tag{2.10}$$

These are already quantities that can be measured. For that reason, it is good to state the definition of M and Δm explicitly.

$$M = (m_H + m_L)/2 \qquad \text{and} \qquad \Delta m = m_H - m_L \tag{2.11}$$

The observations can be made for the neutral mesons that oscillate between their CP-eigenstates. For instance, for the neutral B^0-meson system, the mass difference between the two mesons is $(0.333 \pm 0.001)\,\mathrm{MeV}$ or $(0.5065 \pm 0.0019)\,\mathrm{ps}^{-1}$. [17].
Returning to the wave function, it is now possible to determine the fraction of q over p:

$$H\psi = \Lambda\psi \rightarrow \frac{q}{p} = \sqrt{\frac{M_{12}^* - \frac{i}{2}\Gamma_{12}^*}{M_{12} - \frac{i}{2}\Gamma_{12}}} \tag{2.12}$$

If the Heisenberg formulation of quantum mechanics is now further followed, it is possible to leap towards the oscillations of the mesons in a natural way. Now that p and q are determined, the mass eigenstates of this system can be expressed in terms of a superposition of strong eigenstates:

$$\begin{aligned} |P_H\rangle &= p\,|P^0\rangle + q\left|\overline{P^0}\right\rangle \\ |P_L\rangle &= p\,|P^0\rangle - q\left|\overline{P^0}\right\rangle \end{aligned} \qquad \text{and} \qquad \begin{aligned} |P^0\rangle &= \tfrac{1}{2p}\left[|P_H\rangle + |P_L\rangle\right] \\ \left|\overline{P^0}\right\rangle &= \tfrac{1}{2q}\left[|P_H\rangle - |P_L\rangle\right] \end{aligned} \tag{2.13}$$

Now it is important to note that $|P_H\rangle$ and $|P_L\rangle$ are mass eigenstates, such that their time evolution can be obtained by multiplying them with the corresponding entries in the Hamiltonian:

$$
\begin{aligned}
|P_H(t)\rangle &= e^{-im_H t-\Gamma_H t/2}\,|P_H(0)\rangle \\
|P_L(t)\rangle &= e^{-im_L t-\Gamma_L t/2}\,|P_L(0)\rangle
\end{aligned}
\tag{2.14}
$$

Combining Equations 2.14 and 2.13, the expression given below is obtained for the state $|P(t)\rangle$. Because it is rather involved expression if everything is written explicitly, let us define a shorthand first;

$$
g_{\pm}(t) = \frac{1}{2}e^{-iMt}\left(e^{-i\Delta mt/2-\Gamma_H t/2} \pm e^{+i\Delta mt-\Gamma_L t/2}\right) \tag{2.15}
$$

Now for the expression for $|P(t)\rangle$ and its CP partner:

$$
\begin{aligned}
\left|P^0(t)\right\rangle &= \frac{1}{2p}\left\{e^{-im_H-\Gamma_H t/2}\,|P_H(0)\rangle + e^{-im_L-\Gamma_L t/2}\,|P_L(0)\rangle\right\} \\
&= g_+(t)\left|P^0\right\rangle + \left(\frac{q}{p}\right) g_-(t)\left|\overline{P}^0\right\rangle
\end{aligned}
\tag{2.16}
$$

and

$$
\left|\overline{P}^0(t)\right\rangle = g_-(t)\left(\frac{p}{q}\right)\left|P^0\right\rangle + g_+(t)\left|\overline{P}^0\right\rangle \tag{2.17}
$$

Now as we know from elementary quantum mechanics, we need to take the in-product of the state together with $|P(t)\rangle$ and square it to find the probability for a particle to transform into the other state. An example: if there exists a pure sample of $\left|\overline{P}^0\right\rangle$ particles initially, the probability for finding a $|P^0\rangle$ particle is given by

$$
\left|\left\langle P^0\middle|\overline{P}^0(t)\right\rangle\right|^2 = |g_-(t)|^2\left(\frac{p}{q}\right)^2 \tag{2.18}
$$

Which, happens to be simplifiable to the expression

$$
|g_{\pm}|^2 = \frac{e^{-\Gamma t}}{2}\left(\cosh\left(\frac{1}{2}\Delta\Gamma t\right) \pm \cos(\Delta m t)\right) \tag{2.19}
$$

where

$$
\Gamma = (\Gamma_L + \Gamma_H)/2 \qquad \text{and} \qquad \Delta\Gamma = \Gamma_L - \Gamma_H \tag{2.20}
$$

are used in the same fashion as what was done with the masses.

If the correct parameters for the B^0-mesons are filled in Equation 2.18, it is possible to see the oscillations of the mesons between the two mass eigenstates. This is quite illustrative, because it immediately becomes very clear from the figures that the oscillations play a much larger role for the B_s^0-$\overline{B}_s^0$ system than for the B_d^0-$\overline{B}_d^0$-system. This is also easily observed In Figure 2.3, where the oscillations are visualised for the B^0, B_s^0 and D^0 mesons.

It is clear the mixing-induced CP-asymmetry is much more dominant in the $B_d \to D_d^+ D_d^-$ decay than in the $B_s \to D_s^+ D_s^-$ decay. It is also possible to draw the Feynman diagram of this process; it is a so-called "Box-diagram".

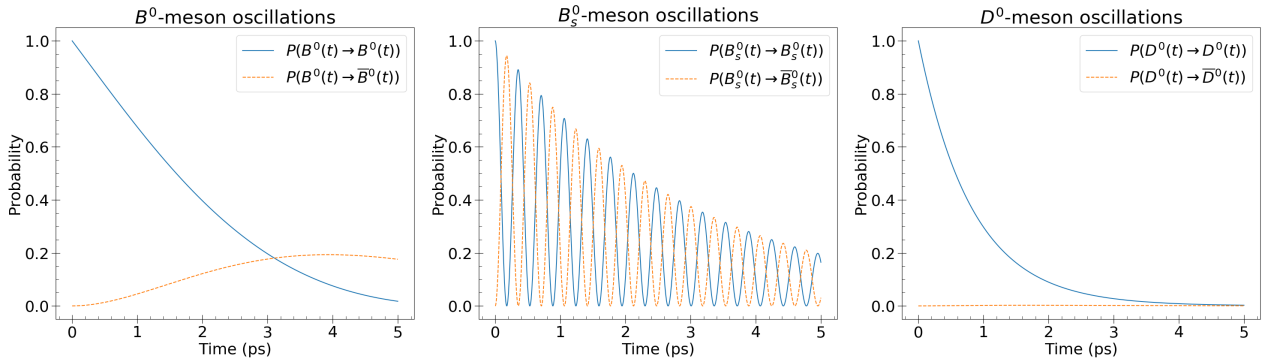

Figure 2.3: The probabilities for observing an antimeson or meson after starting of with a pure $|P^0\rangle$-state.

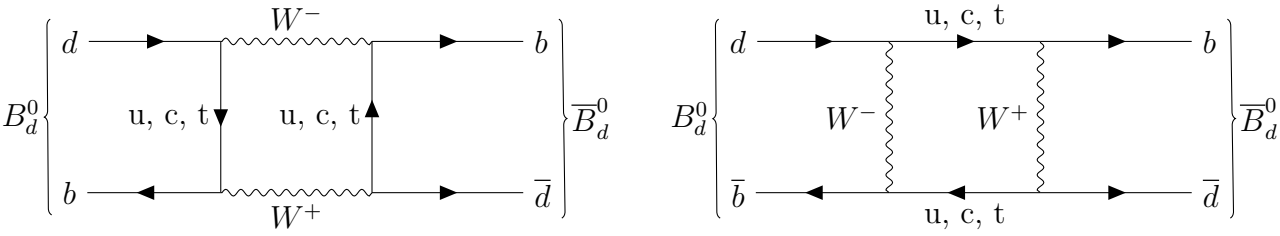

2.5 The CKM-Matrix and the Unitarity Triangles

To be able to implement weak decays and quark mixing into the Standard Model, a mechanism for connecting the three quark generations is required. As was mentioned in the introduction, the CKM-matrix is the mechanism incorporated in the Standard Model that does so.

The mechanism of quark mixing in the Standard Model was already constructed before the observation of CP-violation. Cabibbo devised a 2×2 matrix where the first two generations of quarks could be connected to one another [1]. To allow for the phase that allows for CP-violation, three generations are required. Kobayashi and Maskawa took this thought and further developed Cabibbo's ideas, constructing a 3×3 matrix [2]. This was still before the first top- or beauty quark was found. This 3×3 matrix is called the CKM-matrix. Although this matrix has complex values for each element, which means that there are $3 \times 3 \times 2 = 18$ parameters that can be varied, those can be highly constrained. There is the unitarity ($U^\dagger U = \mathbb{1}$) constraint, which implies that for an $n \times n$ matrix there are n unitary constraints for the diagonal elements and $n^2 - n$ constraints for the off-diagonal elements, as they have to be orthogonal. Finally, the theory is invariant to an overall phase difference in the quark fields, which means that we can rotate away $2n - 1$ of the remaining phases. This leaves us with $2n^2 - n - (n^2 - n) - (2n - 1) = n^2 - 2n + 1$ free parameters. As the CKM-matrix is a 3×3 matrix, there remain $9 - 6 + 1 = 4$ free parameters.

One parametrisation of these constraints is in the form of three Euler angles and a complex phase. This is already an interesting note in itself, as to allow for CP-violation the matrix has to contain a complex phase. When Cabibbo made the first steps towards this parametrisation halfway through the sixties, he only allowed for two generations of quarks. With the constraints that have been considered so far, it is not possible to allow for CP-violation with only the

single free parameter that would be available in that model. Hence, Kobayasho and Maskawa hypothesized that there must be a third generation of quarks and proposed that the matrix should have at least a 3×3 form.
The CKM-matrix can be given as

$$V_{CKM} = \begin{bmatrix} V_{ud} & V_{us} & V_{ub} \\ V_{cd} & V_{cs} & V_{cb} \\ V_{td} & V_{ts} & V_{tb} \end{bmatrix} \tag{2.21}$$

The constraints that we imposed above can also be expressed in matrix form instead of deriving them from group theoretic arguments:

$$V_{CKM}^{\dagger} V_{CKM} = \begin{bmatrix} V_{ud}^* & V_{cd}^* & V_{td}^* \\ V_{us}^* & V_{cs}^* & V_{ts}^* \\ V_{ub}^* & V_{cb}^* & V_{tb}^* \end{bmatrix} \begin{bmatrix} V_{ud} & V_{us} & V_{ub} \\ V_{cd} & V_{cs} & V_{cb} \\ V_{td} & V_{ts} & V_{tb} \end{bmatrix} = \mathbb{1} \tag{2.22}$$

From this product we can see that there are three unitarity relations that have to hold [18]:

$$\begin{aligned} V_{ud}V_{ud}^* + V_{us}V_{us}^* + V_{ub}V_{ub}^* &= 1 \\ V_{cd}V_{cd}^* + V_{cs}V_{cs}^* + V_{cb}V_{cb}^* &= 1 \\ V_{td}V_{td}^* + V_{ts}V_{ts}^* + V_{tb}V_{tb}^* &= 1 \end{aligned} \tag{2.23}$$

Additionally, $V_{CKM}V_{CKM}^{\dagger} = \mathbb{1}$, which results in six more equations.

$$\begin{aligned} V_{ud}V_{cd}^* + V_{us}V_{cs}^* + V_{ub}V_{cb}^* &= 0 \\ V_{ud}V_{td}^* + V_{us}V_{ts}^* + V_{ub}V_{tb}^* &= 0 \\ V_{cd}V_{td}^* + V_{cs}V_{ts}^* + V_{cb}V_{tb}^* &= 0 \\ V_{ud}V_{us}^* + V_{cd}V_{cs}^* + V_{td}V_{ts}^* &= 0 \\ V_{ud}V_{ub}^* + V_{cd}V_{cb}^* + V_{td}V_{tb}^* &= 0 \\ V_{us}V_{ub}^* + V_{cb}V_{cs}^* + V_{tb}V_{ts}^* &= 0 \end{aligned} \tag{2.24}$$

For completeness it should be mentioned that by the nature of the matrix, the complex conjugates of these equations will also hold. These equations do not provide any new information - the parameters will take the same value, up to an overall phase. Since overall phases are not observable, all information is contained in Equation 2.23 and 2.24.
The parametrisation in the form of Euler angles and complex phases can be shown as a product of three Euler-matrices, which form the irreducible representation of SO(3). Because the product of the three matrices cannot be conveniently presented without making any modifications on the length of the expressions, the substitutions $\cos(\theta_{ij}) = c_{ij}$ and correspondingly $\sin(\theta_{ij}) = s_{ij}$ have been made.

$$V_{CKM} =$$

$$= \begin{bmatrix} 1 & 0 & 0 \\ 0 & \cos(\theta_{23}) & \sin(\theta_{23}) \\ 0 & -\sin(\theta_{23}) & \cos(\theta_{23}) \end{bmatrix} \begin{bmatrix} \cos(\theta_{13}) & 0 & \sin(\theta_{13})e^{-i\delta_{13}} \\ 0 & 1 & 0 \\ -\sin(\theta_{13})e^{i\delta_{13}} & 0 & \cos(\theta_{13}) \end{bmatrix} \begin{bmatrix} \cos(\theta_{12}) & \sin(\theta_{12}) & 0 \\ -\sin(\theta_{12}) & \cos(\theta_{12}) & 0 \\ 0 & 0 & 1 \end{bmatrix}$$

$$= \begin{bmatrix} c_{12}c_{13} & s_{12}c_{13} & s_{13}e^{-i\delta_{13}} \\ -s_{12}c_{23} - c_{12}s_{23}s_{13}e^{-i\delta_{13}} & c_{12}c_{23} = s_{12}s_{23}s_{13}e^{i\delta_{13}} & s_{13}e^{i\delta_{13}} \\ s_{12}s_{23} - c_{12}c_{23}s_{13}e^{i\delta_{13}} & -c_{12}s_{23} - s_{12}c_{23}s_{13}e^{i\delta_{13}} & c_{13}c_{13} \end{bmatrix} \tag{2.25}$$

The CKM-matrix with Euler angles, as shown in Equation 2.25, is not very convenient to take into account while performing computations; numerical evaluations of trigonometric functions are both computationally expensive and prone to human errors in setting them up. Therefore it would be beneficial to find a simpler representation. A good representation was devised by Lincoln Wolfenstein in 1983 [19]. From observations it was already known that the diagonal elements of the matrix were close to unity, where the off-diagonal elements were a lot smaller. The sizes of the CKM-matrix elements can be measured through various decay reactions. The element V_{ud} for example can be measured through a specific β-decay where the nucleus remains at a state of positive parity and no spin by emission of two particles with opposite spin; the $0^+ \rightarrow 0^+$ transition. This gives $V_{ud} = 0.97420 \pm 0.00021$ [20], as opposed to $|V_{us}| = 0.2245 \pm 0.0005$ as determined mainly from Kaon and Pion decay constants in $K \rightarrow \mu\nu(\gamma)$ and $\pi \rightarrow \mu\nu(\gamma)$ averaged in Section 66 of [17] and $|V_{ub}| = (3.94 \pm 0.36) \times 10^{-3}$ as determined from $B \rightarrow X_u l\bar{\nu}$ decays by CLEO, BaBar and Belle, among others, averaged in Section 75 of [17]. A similar trend is found for other elements; the farther away the matrix elements are from the diagonal, the smaller the contribution of that element to the mixing matrix. A visual comparison of the sizes of the matrix elements is shown in Figure 2.5.
The coupling through the diagonal elements is stronger than that of the off-diagonal elements, which allows for an expansion in terms of the Euler angle. Mathematically, this is done by taking the value $\lambda = |V_{us}|$ as an expansion parameter. Also, since $\sin(\theta_{13})$ and $\sin(\theta_{23})$ are very close to 0 (within 10^{-3} and 10^{-2}), $\cos(\theta_{13})$ and $\cos(\theta_{23})$ are set to 1.

$$\sin(\theta_{12}) = \lambda \Rightarrow \cos(\theta_{12}) = \sqrt{1-\lambda^2} \xrightarrow{\text{T. E.}} 1 - \frac{\lambda^2}{2} + \mathcal{O}(\lambda^4) \tag{2.26}$$

When the same method is employed for all the angles involved, setting

$$\sin(\theta_{12}) = \lambda, \sin(\theta_{23}) = A\lambda^2, \sin(\theta_{13})e^{-i\delta_{13}} = A\lambda^3(\rho - i\eta) \tag{2.27}$$

the following result is obtained. The parameter λ is found to be best approximated with $\lambda = 0.2245 \pm 0.0005$. [17]. Comparing Equation 2.25 and 2.28 it is clear that the latter

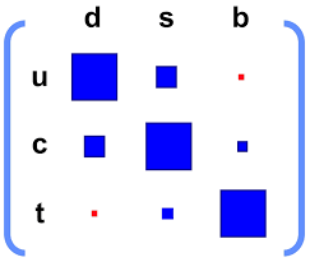

Figure 2.5: The relative sizes of the CKM elements visualized as the areas of the squares

is far easier to work with. When formulating this expression for the CKM-matrix, Wolfenstein also proved that the constraints that were imposed before are also still valid, up to $\mathcal{O}(\lambda^4)$.

$$V_{CKM} = \begin{bmatrix} 1-\frac{1}{2}\lambda^2 & \lambda & A\lambda^3(\rho - i\eta) \\ -\lambda & 1-\frac{1}{2}\lambda^2 & A\lambda^2 \\ A\lambda^3(1-\rho-i\eta) & -A\lambda^2 & 1 \end{bmatrix} + \mathcal{O}(\lambda^4) \tag{2.28}$$

Looking at the equations that arise from the unitary constraint in Equation 2.24 on the CKM-matrix and the Wolfenstein parametrisation, an interesting observation can be made. Substituting the Wolfenstein parametrisation into the equations, in particular the fifth one, gives the expression in Equation 2.29. This relation in particular is interesting, because all of the terms have approximately the same length; unnormalised, all edges have a length that is proportional to $A\lambda^3$. The other relations have terms that are dependent on different orders of λ.

$$V_{ud}V_{ub}^* + V_{cd}V_{cb}^* + V_{td}V_{tb}^* = 0 \rightarrow 1 + \frac{V_{cd}V_{cb}^*}{V_{ud}V_{ub}^*} + \frac{V_{td}V_{tb}^*}{V_{ud}V_{ub}^*} \tag{2.29}$$

As all the terms in this equation are complex numbers, they can be visualised in a complex plane as being a triangle. This triangle is shown in Figure 2.6. The angles of this unitarity triangle can be determined experimentally by performing measurements on processes that involve the corresponding matrix elements of the CKM-matrix. It is conventional to renormalise the sides by a factor of $\frac{1}{V_{ud}V_{ub}^*}$. The enclosed angles of the triangle can be defined through

$$\alpha = \arg\left(-\frac{V_{td}V_{tb}^*}{V_{ud}V_{ub}^*}\right), \beta = \arg\left(\frac{V_{td}V_{tb}^*}{V_{cd}V_{cb}^*}\right), \gamma = \arg\left(-\frac{V_{ud}V_{ub}^*}{V_{cd}V_{cb}^*}\right) \tag{2.30}$$

The angle α can be measured by measuring the CP-asymmetries in the decay of B-mesons to $\pi^+\pi^-$, $\rho^+\pi^-$, and ρ^+ and ρ^- [21]. The angle β can be measured by studying the oscillations in the neutral B-meson system [8] and the angle γ is determined through the $B^0 \rightarrow D^+\pi^-$ decays, among others [22].

Besides the triangle shown in Figure 2.6, another triangle from the unitarity constraints to the CKM-matrix is relevant. This is the triangle that includes the elements that are relevant for the $B_s \rightarrow D_s^+D_s^-$ decay. To give a better idea of the triangles themselves not obfuscated with measurements, both the Unitarity Triangle and the triangle relevant for the $B_s \rightarrow D_s^+D_s^-$ decays are shown in Figure 2.7a and 2.7b. These triangles are also used to define the phases ϕ_d and ϕ_s. These angles are the CP-violating phases in the meson mixing process that can be derived from the Standard Model; they can be closely related to the dispersive and absorptive parameters M_{12} and Γ_{12} in the B^0- or B_s^0-meson oscillations. The ϕ_d is connected to the angles shown in Equation 2.30 through

$$\phi_d = 2\beta \tag{2.31}$$

Through one of the other unitarity relations, it is possible to define ϕ_s. Analogous to the previous case, the relevant angle here is β_s. The angle β_s is written as

$$\beta_s = \arg\left(-\frac{V_{ts}V_{tb}^*}{V_{cs}V_{cb}^*}\right) \tag{2.32}$$

and just as before, it relates to ϕ_s through the identity

$$\phi_s = -2\beta_s \tag{2.33}$$

Not only the angles in the triangle are useful quantities to define. Where the argument of the terms in Equation 2.29 can be used to define the angles of the triangle, the absolute value of the terms are the lengths of the vertices of the triangles. The important vertex for this research is the vertex that is denoted R_b in Figure 2.7a. The definition of this vertex and

$$R_b = \left|\frac{V_{ud}V_{ub}^*}{V_{cd}V_{cb}^*}\right| = 0.410 \pm 0.030 \tag{2.34}$$

This number is based on averages for the elements in the CKM-matrix given by the Particle Data Group in [23]. These averages are based on measurements of multiple groups with different methodologies for determining the CKM-elements. The values used to compute R_b here are

$$\begin{aligned} V_{ud} &= 0.97370 \pm 0.00014 \quad & V_{ub} &= (3.82 \pm 0.24) \times 10^{-3} \\ V_{cd} &= 0.221 \pm 0.004 & V_{cb} &= (41 \pm 1.4) \times 10^{-3} \end{aligned} \tag{2.35}$$

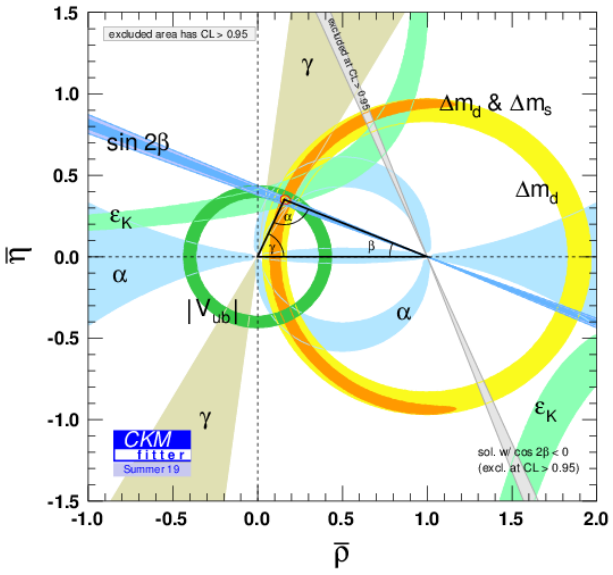

Figure 2.6: Current constraints on the unitarity triangle. Taken from the CKMFitter group, [24]

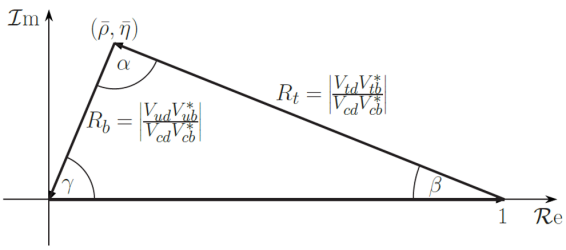

(a) The unitarity triangle from the relation that defines β, which relates to ϕ_d. Taken from [8].

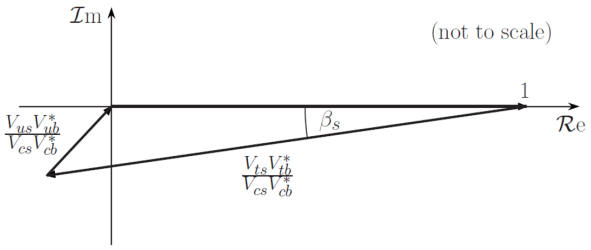

(b) The unitarity triangle from the relation that defines β_s, which relates to ϕ_s. Taken from [8].

Figure 2.7: The triangles produced by the unitarity constraints on the CKM-matrix.

2.6 Penguin diagrams and Related Decay Topologies

The Feynman diagrams that can be drawn for a process directly relate to the amplitude of that process. By calculating the contribution of all processes with different decay topologies, it is possible to determine the total amplitude of that process. The word topology is used here to indicate the different ways of connecting all contributing lines in the Feynman diagrams. As the particles interact with each other at different points, the intermediate process is slightly different while the final state will still be the same. The relevant decay topologies here will be the Tree and Penguin diagram. The Tree diagram is the easiest one to define. These diagrams contain no loops and have the same shape a the trees often represented in Graph theory. External branches coincide into a vertex, there is a possible internal line leading to another vertex, and two or more particles depart from that vertex.

There exist two different types of Tree diagrams: the colour-allowed and colour-suppressed form [25]. Tree diagrams that are colour-allowed have the quark-antiquark pair produced by the W-boson end up in the same meson, because these quarks have been created as a colour-singlet. When the quark-antiquark pair ends up in two different mesons, the Tree diagram is colour-suppressed because there are less colour combinations for the quark-antiquark pair to combine with the final- and spectator quark, reducing the amplitude of the diagram.

The CP-asymmetries that are used as observables originate from the CP-violating phase in the CKM-matrix of the Standard Model, but they can be used to measure the contribution of the Penguin diagrams in B-meson decays [26]. Penguin diagrams are another class of Feynman diagram where an internal loop is involved. The b-quark in the B-meson will temporarily change flavour, and the intermediate W-boson or the virtual quark will participate in an interaction. That particle will later be reabsorbed, but the products from that interaction are still available to end up in the final state of the diagram.

Based on these constraints given in the previous paragraph there are two different diagrams that can be drawn: the regular Penguin diagram (Figure 2.8b) and the Penguin Annihilation diagram. For the regular Penguin diagram, the spectator quark does not participate in the interaction process. The W-boson is reabsorbed by what previously was the b-quark. In the Penguin Annihilation diagram the b- and spectator quark in the B-meson annihilate during the exchange of a W-boson into a state of gluons. There have to be at least two gluons due

to constraints on the colour charges. These gluons then create the two quark-antiquark pairs that make up the D-mesons.

The Penguin Annihilation diagram (Figure 2.8d) will not be considered here, because the final state and the initial state are only connected by gluon lines. When a Feynman diagram can be split into two separate diagrams by cutting a single gluon line where the original- and final state particles are separated, the diagram is OZI-suppressed. The theory of OZI-suppression (after Okubo, Zweig, and Iizuka) [27] is based on the fact that the coupling of the strong force gets weaker for higher energies. In the case of the penguin annihilation diagram that can be seen because the energy of the gluons is at least equal to the energy of the two quarks in the B-meson.

There is also the Exchange topology (Figure 2.8c), where the b-quark and the spectator quark (which at this point is not really a spectator anymore) interact through a virtual W-boson. The remainder of the energy is used for the creation of the $d\overline{d}$ or $s\overline{s}$ pair.

To complete the list it is also needed to introduce the Annihilation diagram. The Annihilation does not contribute to the $B_d \to D_d^+ D_d^-$ or $B_s \to D_s^+ D_s^-$ decay, but it is relevant for $B^+ \to \overline{D^0} D_{(s/d)}^+$ for example. It is easy to see why: in this diagram the constituent quarks of the B-meson annihilate into a W-boson, which transitions into a u and d or s. As the W boson carries a charge of ± 1, this process cannot occur for neutral B-mesons.

If the Feynman diagram is considered as a calculational tool, it is known that diagrams with more loops are higher order diagrams contribute less to the amplitude of the process than the tree diagram for the same process. In the decays that are considered in this thesis, the Penguin diagrams will always be a correction to the tree diagrams. There are however processes where the tree topology is not allowed, such that the Penguins are in fact the dominant contribution. An example of this is the $B \to \phi\phi$ decay [28]. For $B_d \to D_d^+ D_d^-$ and $B_s \to D_s^+ D_s^-$ however this is not the case.

Having discussed all of the relevant diagrams, it is possible to compare the transitions for the $B_q \to D_q^- D_q^+$ process and that of $B \to J/\psi X$ decays, as depicted in Figure 2.9. The latter family of decays has also been used to analyse the shift $\Delta\phi_s$. In the latter process, the quark-antiquark pair that is produced ends up in a single meson: the J/ψ-meson. This meson is a form of charmonium, composed of a charm- and anticharm quark ($c\overline{c}$). In the $B_q \to D_q^- D_q^+$ the two c-quarks are split over the two charmed D-mesons. The same diagrams described above also apply to this family of decays, which makes the results obtained from the $B_q \to D_q^- D_q^+$ a good check of what is seen there.

It is assumed that the exchange topology and the penguin annihilation topology do not contribute significantly to the total decay amplitude of the process [25], however in recent findings there exist arguments that speak against ignoring these contributions completely [26]. However, considering contribution of smaller orders only becomes productive when the contributions from larger orders are taken care of. For that reason, the Penguin Annihilation, Exchange, and Annihilation diagrams will be ignored.

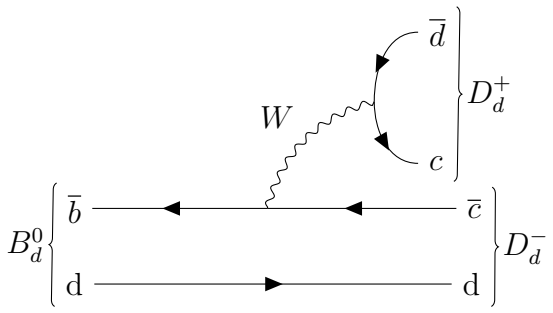

(a) The tree topology (T)

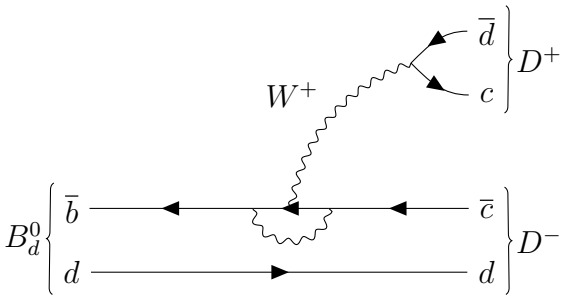

(b) The penguin topology (P)

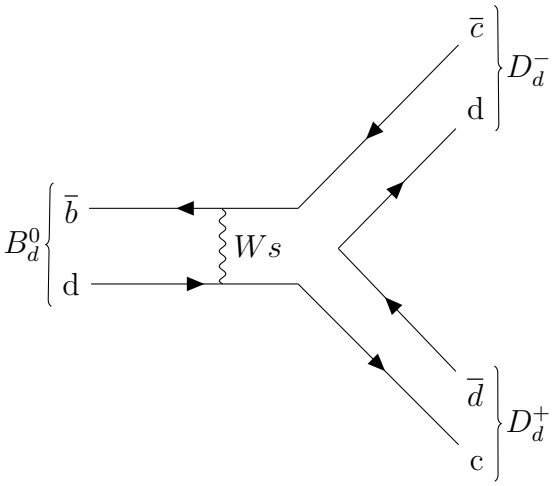

(c) The exchange topology (E)

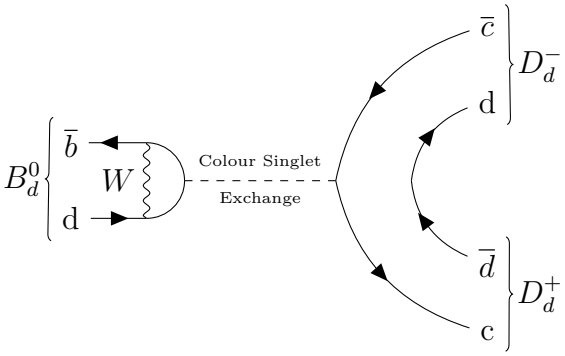

(d) The penguin annihilation topology (PA)

Figure 2.8: All relevant different decay topologies for the $B_q \to D_q^- D_q^+$ decay. If the d-quark is interchanged for an s-quark, the diagrams for $B_s \to D_s^+ D_s^-$ are obtained.

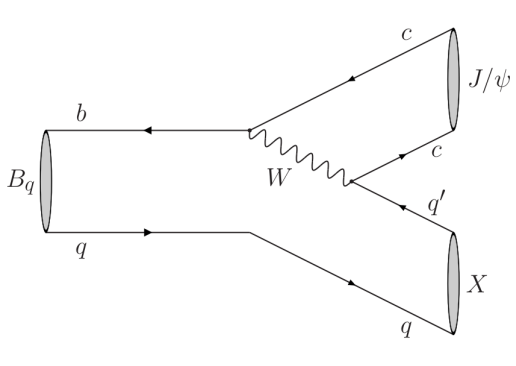

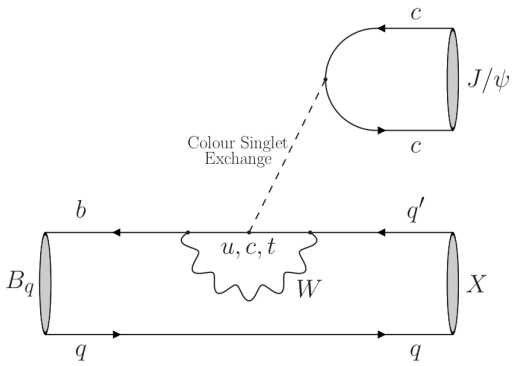

Figure 2.9: Illustration of the Tree and Penguin diagram contributing to the $B_q \to J/\psi X$ decay channels. Taken from [8]

2.7 Decay Amplitudes and Observables

Computing the analytic expression for these Feynman diagrams that describe these processes is not easily done, as the hadronic parameters that appear in the amplitude are difficult to quantize. It is also important to note that the diagrams that are given in Figure 2.8 are the general versions of the topologies; the internal lines in the Penguin or Penguin Annihilation diagram can be an up-, charm-, or top-quark. Those topologies hence code for three different topologies each.

There is still a way to compare these diagrams to each other. When the contributions of the topologies to the amplitudes are written out, it is possible to reshape them such that the two expressions are quite similar [29].

$$\begin{aligned}\mathscr{A}(B_d \to D_d^+ D_d^-) &= V_{ud}V_{ub}^* P^{(u)} + V_{td}V_{tb}^* P^{(t)} + V_{cd}V_{cb}^* \left(P^{(c)} + T\right) \\ &= \left(1 - \frac{\lambda^2}{2}\right) A\lambda^3(\rho + i\eta)P^{(u)} + A\lambda^3(1 - \rho - i\eta)P^{(t)} - A\lambda^3 \left(P^{(c)} + T\right) \\ &= -\mathcal{A}\lambda \left[1 - ae^{i\theta}e^{i\gamma}\right]\end{aligned} \tag{2.36}$$

Where the hadronic parameters $\mathcal{A}$ and $ae^{i\theta}$ are given by Equation 2.37. The parameter a signifies the relative contribution from the penguin diagrams. The parameter θ in this expression is the strong phase difference between the terms. Finally, γ stands for the weak phase difference [24]. This is also the angle γ from the Unitarity Triangle.

$$\begin{aligned}\mathcal{A} &\equiv \lambda^2 A \left[T + P^{(c)} - P^{(t)}\right] \\ ae^{i\theta} &= R_b \left[\frac{P^{(u)} - P^{(t)}}{T + P^{(c)} - P^{(t)}}\right]\end{aligned} \tag{2.37}$$

A similar strategy can be performed to express the amplitude for the $B_s \to D_s^+ D_s^-$ decay, although a slightly different result will be obtained. Because the penguin parameters for this decay are for a different process, they will be appended with a prime. In the following equation, the definition

$$\epsilon \equiv \frac{\lambda^2}{1 - \lambda^2} = 0.0536 \pm 0.0003 \tag{2.38}$$

is used.

$$\mathscr{A}(B_s \to D_s^+ D_s^-) = \left(1 - \frac{\lambda^2}{2}\right) \mathcal{A}' \left[1 + \epsilon a' e^{i\theta'} e^{i\gamma}\right] \tag{2.39}$$

It is important to note here that the leading order terms for the decay of the B_s and B_d meson are different. The decay amplitude for $B_s \to D_s^+ D_s^-$ is two orders lower in λ, which means that the overall decay is enhanced with respect to $B_d \to D_d^+ D_d^-$. However, the term ϵ in the expression makes it that the penguin contributions for this decay are suppressed by approximately 20 times [29]. The fact that the penguin diagrams here are suppressed by such a large factor, makes it difficult to determine them accurately. It is not possible to compute them from first principles, and by this reduction to the amplitude of the decay process it is difficult to perform a statistically significant analysis. To circumvent this problem, it is possible to assume that the $SU(3)_F$ flavour symmetry of the Standard Model treats the QCD-interactions in the $B_d \to D_d^+ D_d^-$ and $B_s \to D_s^+ D_s^-$ decays as the same, and that therefore the penguin parameters a and θ are the same. Therefore, in this thesis, it will be assumed that

$$ae^{i\theta} = a'e^{i\theta'} \qquad \text{and} \qquad \mathcal{A} = \mathcal{A}' \tag{2.40}$$

The CP-asymmetries can be measured by observing the decay products from the B-meson and its CP-partner $\overline{B}$ [30]. If the CP-observables are determined in this manner, it can be related to the decay rate:

$$a_{CP}(t) = \frac{\Gamma(B_d \to D_d^+ D_d^-)(t) - \Gamma(\overline{B_d} \to D_d^+ D_d^-)(t)}{\Gamma(B_d \to D_d^+ D_d^-)(t) + \Gamma(\overline{B_d} \to D_d^+ D_d^-)(t)} \tag{2.41}$$

where Γ is the decay width of the reaction and the asymmetry is time-dependent because of the meson-antimeson oscillations. The decay width of the reactions are the squared amplitude of the process. An initial B_d^0 meson evolves over time into a linear combination of B_d^0 and $\overline{B_d^0}$ states. As the decay widths are directly related to the amplitudes of the decay processes, where these in turn are related to the asymmetries, this asymmetry can be written as

$$a_{CP}(t) = \frac{A_{CP}^{Dir}(B_d \to D_d^+ D_d^-)\cos(\Delta m t) + A_{CP}^{Mix}(B_d \to D_d^+ D_d^-)\sin(\Delta m t)}{\cosh(\Delta\Gamma t/2) + A_{\Delta\Gamma}(B_d \to D_d^+ D_d^-)\sinh(\Delta\Gamma t/2)} \tag{2.42}$$

The parameters Δm and $\Delta\Gamma$ relate to the properties derived before, in Equations 2.11 and 2.20. The three CP-observables used in Equation 2.42 are [31]:

$$A_{CP}^{Dir}(B_q \to D_q^- D_q^+) = \frac{2b_q \sin(\rho_q)\sin(\gamma)}{1 - 2b_q\cos(\gamma) + b_q^2} \tag{2.43}$$

$$A_{CP}^{Mix}(B_q \to D_q^- D_q^+) = \eta_q \left[\frac{\sin(\phi_q) - 2b_q\cos(\rho_q)\sin(\phi_q+\gamma) + b_q^2\sin(\phi_q+2\gamma)}{1 - 2b_q\cos(\rho_q)cos(\gamma) + b_q^2}\right] \tag{2.44}$$

$$A_{\Delta\Gamma}(B_q \to D_q^- D_q^+) = -\eta_q \left[\frac{\cos(\phi_q) - 2b_q\cos(\rho_q)\cos(\phi_q+\gamma) + b_q^2\cos(\phi_q+2\gamma)}{1 - 2b_q\cos(\rho_q)\cos(\gamma) + b_q^2}\right] \tag{2.45}$$

where the substitution is made for the parameters in Equations (2.43 - 2.45) depending on what decay amplitude is being studied. The substitutions are:

$$B_d \to D_d^+ D_d^- : b_d e^{i\rho_d} = a e^{i\theta} \qquad \text{and} \qquad B_s \to D_s^+ D_s^- : b_s e^{i\rho_s} = -\epsilon a' e^{i\theta'} \tag{2.46}$$

The η_q in Equations 2.44 and 2.45 represents the CP-eigenvalue of the final state. In case of the D^+D^-- or $D_s^+D_s^-$-state, these both amount to $\eta_d = \eta_s = +1$. The D-mesons are CP-partners, such that $CP\left|D_q^+\right\rangle = \left|\overline{D_q^-}\right\rangle$.

Now being aware of all the necessary theoretical prerequisites, it is time to develop a better intuition on ϕ_d and ϕ_s. These parameters have Standard Model prediction values, $\phi_d = 2\beta = (44.28 \pm 1.40)°$ and $\phi_s = -2\beta_s = (-2.15 \pm 0.11)°$. ϕ_q represents the mixing phases in the $B_q^0 - \overline{B_q^0}$ system. This phase can be measured by measuring the CP-violating observables resulting from the $B_q \to D_q^- D_q^+$ decays. The Penguin diagrams introduce an additional shift in this parameter ϕ_d and ϕ_s. These shifts will be denoted by $\Delta\phi_d$ and $\Delta\phi_s$. The shift due to the Penguin diagrams result in the fact that the measured value for ϕ_d and ϕ_s will differ from the Standard Model prediction. The actual measurement for ϕ_s will be build up as

$\phi_s^{eff} = -2\beta_s + \Delta\phi_s$, and similarly for ϕ_d.
Remember that the first two CP-observables have different sources; A_{CP}^{Dir} is caused by the interference between the tree and penguin topologies, while the the observable A_{CP}^{Mix} comes from the interference between $B-\overline{B}$-mixing and the decay to the charmed mesons [8]. Note that this also means that there can be no direct CP-asymmetry when the penguins do not contribute to the decay; A_{CP}^{Dir} would then be identically zero. The mixing asymmetry is dependent on the weak phase $\phi_{d/s}$. This also indicates how it is possible to measure the shift induced by the penguin diagrams in the parameters $\phi_{d/s}$.
Another interesting observation can be made here. There exists a certain degeneracy in the values for the Penguin parameters shown in Equation 2.46. When the amplitudes in Equation 2.36 and Equation 2.39 are inspected, it can be seen that the amplitudes are invariant under the transformation $a \to -a$ and $\theta = 2\pi - \theta$. The definition that $a > 0$ is maintained throughout this thesis, but the numerical fits may because of this reason show solutions that we do not consider to be relevant.
From fits of the unitarity triangle, as discussed around Figure 2.6, it is possible to determine the angle β. Now it is convenient to define an effective mixing phase

$$\phi_q^{eff} \equiv \phi_q + \Delta\phi_q \tag{2.47}$$

The effective phase can then also be expressed in the CP-observables: [32]

$$\sin\left(\phi_q^{eff}\right) = \frac{A_{CP}^{Mix}(B_q \to D_q^- D_q^+)}{\sqrt{1 - \left(A_{CP}^{Dir}(B_q \to D_q^- D_q^+)\right)^2}} \tag{2.48}$$

The phase shifts $\Delta\phi_d$ and $\Delta\phi_s$ can even be given in terms of the penguin parameters directly. These are very useful relations, as these allow determination of the phase shift directly from the penguin parameters.

$$\Delta\phi_d = \arctan\left(\frac{-2a\cos(\theta)\sin(\gamma) + a^2\sin(2\gamma)}{1 - 2a\cos(\theta)\cos(\gamma) + a^2\cos(2\gamma)}\right) \tag{2.49}$$

$$\Delta\phi_s = \arctan\left(\frac{2\epsilon a'\cos(\theta')\sin(\gamma) + \epsilon^2 a'^2\sin(2\gamma)}{1 + 2\epsilon a'\cos(\theta)\cos(\gamma) + \epsilon^2 a'\cos(2\gamma)}\right) \tag{2.50}$$

Chapter 3

Data Analysis and Results

3.1 Software

The data analysis done for this thesis was done by making use of the GammaCombo software [33]. GammaCombo is built on top of the ROOT framework that was built by the CERN collaboration [34] and is used to perform an analysis of the measurements and the underlying theoretical description to be able to fit the corresponding likelihood functions for the desired parameters of the theory. The program is also able to combine multiple measurements that are dependent on the same parameters and solve for the most probable values of these parameters in the form of a likelihood contour. The method used here is that of overlapping respective probability density functions, such that the resulting probability density function gives a better estimate of the parameters then one of the individual measurements. A visual representation of the process is given in Figure 3.1.

GammaCombo makes use of the log-likelihood method. If the likelihood of one of the individual parameters is given as $\mathcal{L}_i(x_j)$, then the combined likelihood function of all measurements is $\mathcal{L}(x_j) = \prod_i \mathcal{L}_i(x_j)$. To find the best estimate for a parameter x_j, a fitting procedure based on the χ^2-analysis is used. To be able to to this, it is required to define the χ^2-function

$$\chi^2(x_j) = -2\ln\left(\mathcal{L}(x_j)\right) \tag{3.1}$$

If all parameters are assumed to be distributed according to a Gaussian, then the contour intervals can be computed by the probability that $\Delta\chi^2 = \chi(x_j)^2 - \chi(x'_j)^2$ can be exceeded for a one degree of freedom-χ^2-distribution:

$$1 - CL = \frac{1}{\sqrt{2}\Gamma(1/2)} \int_{\Delta\chi^2}^{\infty} e^{-t/2} t^{-1/2} dt \tag{3.2}$$

Here $\Gamma(1/2)$ is the gamma function, the analytic extension of the factorial function over the field of complex numbers [36]. The right hand side of this equation represents the integrated probability for a χ^2-distribution. The contour levels that are predominantly used here are the confidence levels of 39% and 87%.

To analyse the dependence of an observation on two parameters, two-dimensional contours can be drawn. These two-dimensional shapes can be visualised by determining the confidence levels

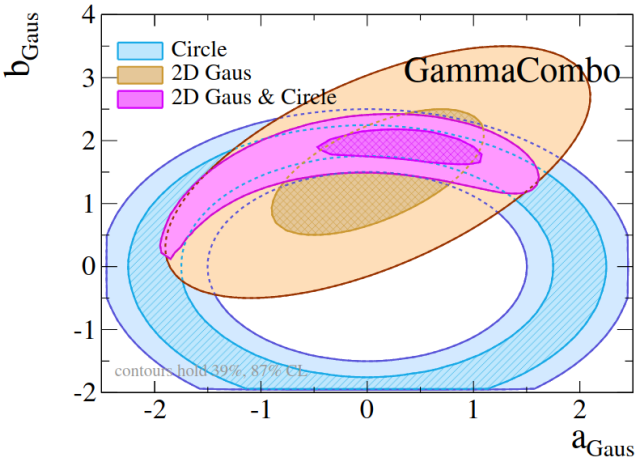

Figure 3.1: The two Gaussian probability distribution functions are plotted in orange and blue. The product of these two functions is again a Gaussian, but it is apparent that this contour is more constrained than its two components. [35]

for parameter x_2 for every inspected value of x_1. It can be seen as slices of the confidence levels of x_2 for varying values of x_1 stacked together. At all of these points, the parameters that are not shown are optimised as well and given as a numerical output by the program.
The bounds for which the probabilities are computed are programmed in the GammaCombo software. This is useful, as we can often define hard boundaries for parameters because of their relation to the physical world. An example is that we limit for the penguin parameter a to $[0, 1]$, as one of the assumptions is that it is a corrective term - that means smaller than R_b as defined in Equation 2.37, which was given with a numerical value of $R_b = 0.410 \pm 0.030$. Giving GammaCombo a range of $[0, 1]$ to confine itself to thus is reasonable. Another reason to constrain ourselves to this domain is that most literature also uses these boundaries making it easier to compare results.

3.2 Determining the Penguin Parameters a, θ, and ϕ_d

To determine the parameters a and θ from measurements, the truth relations in GammaCombo are implemented that represent Equations 2.43 and 2.44. The truth relations tell GammaCombo analytically how the observable varies with the depending parameters. Following that, multiple measurements are imported. These measurements were performed by LHCb [37], BaBar [38] and Belle [39], [40]. The average of these measurements resulted in

$$A_{CP}^{Dir}(B_d \to D_d^+ D_d^-) = -0.23 \pm 0.10 \qquad \text{and} \qquad A_{CP}^{Mix}(B_d \to D_d^+ D_d^-) = 0.77 \pm 0.13 \tag{3.3}$$

The observation for A_{CP}^{Mix} also directly relates to ϕ_d^{eff}, through the relation

$$A_{CP}^{Mix}(B_d \to D_d^+ D_d^-) = \eta_f \sin\left(\phi_d^{eff}\right) \tag{3.4}$$

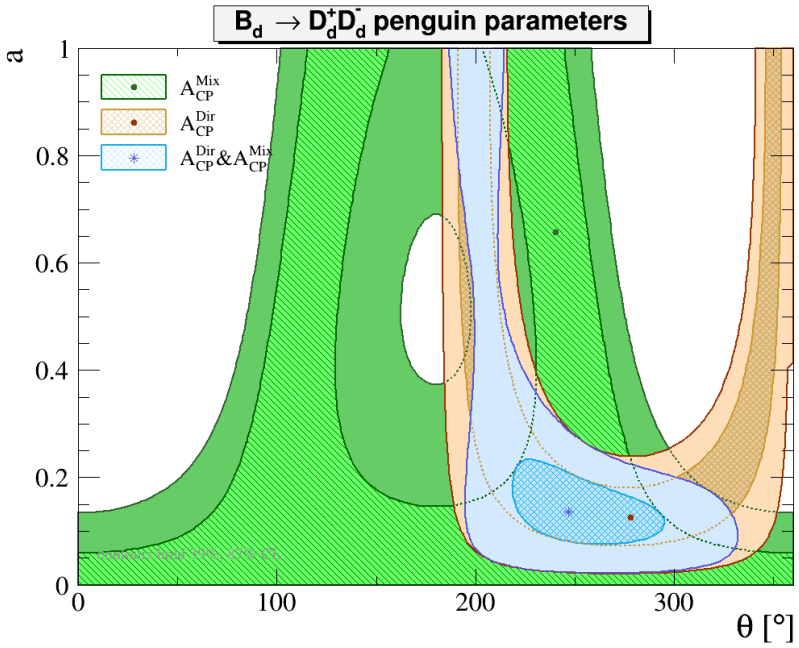

Figure 3.2: The fitted contours for the penguin parameters for the $B_d \to D_d^+ D_d^-$ decay.

When this is combined with the determined value of $\gamma = \left(71.1^{+4.6}_{-5.3}\right)^\circ$ from the HFLAV-group [41] and the external input parameters of

$$\phi_d = (44.28 \pm 1.4)^\circ \tag{3.5}$$

taken from [9], it is possible to solve for the Penguin parameters and show the results in the contour diagram as in Figure 3.2. The observables A_{CP}^{Mix} and A_{CP}^{Dir} both describe a contour depicting the confidence intervals for a and θ based on the programmed truth relation. The intersection of these contours consequently gives the best estimate for these parameters. The best estimates for the penguin parameters are

$$a = 0.147 \pm 0.096 \qquad \text{and} \qquad \theta = (242 \pm 44)^\circ \tag{3.6}$$

Looking at this figure, several observations can be made. Estimates for the value of a and θ have been made, resulting in values for a of approximately 0.1. If the region in Figure 3.2 is considered where a lies around that value, no constraint on θ is put by solely investigating the mixing asymmetry. Drawing the contour for the direct CP-asymmetry is expected to provide clarity, because it is not expected that this asymmetry displays the same behaviour. The phase θ in Equation 2.43 shows which of the two decays ($B_d \to D_d^+ D_d^-$ or $\overline{B_d} \to D_d^- D_d^+$) has the stronger decay width.

A reasonable remark would be to say that the combined fit does not only give a solution near the $a \approx 0.1$ region, but also runs upwards of $a = 1$. Although this indeed turns out to be a numerical possibility, it is important to realise what that means physically. In the theory section, an explanation was given regarding the expectation that the relative amplitude of the penguin diagrams a was only a small correction to the total amplitude, which mainly consists of the tree diagram. If the solution with $a > 1$ is correct, that would mean that the penguin

diagrams are in fact dominant over the tree diagram, which is known to be not the case. In fact, keeping Equation 2.37 in mind, this is the exact reason that we expect that $a < R_b$, as the relative topologies represented in a are suppressed.
Although the arguments given in the previous paragraph already indicate why the solution with $a < R_b$ is preferred, an evidence-based solution is required to confirm. It would be possible to do this by adding more decay channels to this figure; for instance the $B_s \to D_s^+ D_s^-$ channel based on the $SU(3)$-symmetry. This does introduce the problem that ϕ_s is then also required as an input for the fit, but it would remove the ambiguity in the solution.

The penguin parameters in 3.6 result in a phase shift of

$$\Delta\phi_d = (0.14 \pm 0.20)\,\text{rad} = (8 \pm 11)^\circ \tag{3.7}$$

Now to check the performed analysis, it is possible to complete the circle and derive the corrected value ϕ_d^{corr} using the CP-observables and the obtained shift. If everything is working as expected, this should produce the external input for ϕ_d, as seen in Equation 3.5. To determine ϕ_d^{corr}, Equation 2.48 is used. This results in a value of $\phi_d^{eff} = (0.91 \pm 0.20)\,\text{rad}$. Subtracting the determined correction from the penguin diagrams from this value to get back to the external input gives as a result $\phi_d^{corr} = (0.77 \pm 0.20)\,\text{rad} = (44 \pm 11)^\circ$. This is the same number that was used as an external input, except for some missing decimals. This is expected, as from the precision of the Penguin Parameters it is not possible to produce as many significant digits. The fact that this results brings us back to our initial parameters is a good check of the code and computations used in this analysis and strengthens our belief in the validity of the results.

3.3 Making the Step towards ϕ_s

To make the step towards determining the phase shift $\Delta\phi_s$ and the corresponding phase ϕ_s that represents the Standard Model parameter, the penguin parameters that were determined earlier are used. Determining the penguin parameters a' and θ' directly from observables of the $B_s \to D_s^+ D_s^-$ decay is not a feasible solution, as the penguin topologies are suppressed by an extra factor of ϵ. The sensitivity to the penguin topologies should be significantly larger to be able to detect them directly. One could try to determine the angle and its correction while assuming that the measurement value ϕ_s^{corr} is equal to the Standard Model value ϕ_s, but the results obtained in that manner no longer give the required precision and makes the reasoning of obtaining the phase shift in ϕ_s^{eff} circular. Also, the CP-observables for the $B_s \to D_s^+ D_s^-$ decay have not been published directly. They can however be obtained by performing a transformation on the given parameters, which are λ and ϕ_s as measured by LHCb [42]:

$$\phi_s^{eff} = 0.02 \pm 0.17(\text{stat}) \pm 0.02\ (\text{syst})\ \text{rad} \qquad \text{and} \qquad |\lambda| = 0.91^{+0.18}_{-0.15}(\text{stat}) \pm 0.02\ (\text{syst}) \tag{3.8}$$

To translate these to the CP-observables, we use the equations

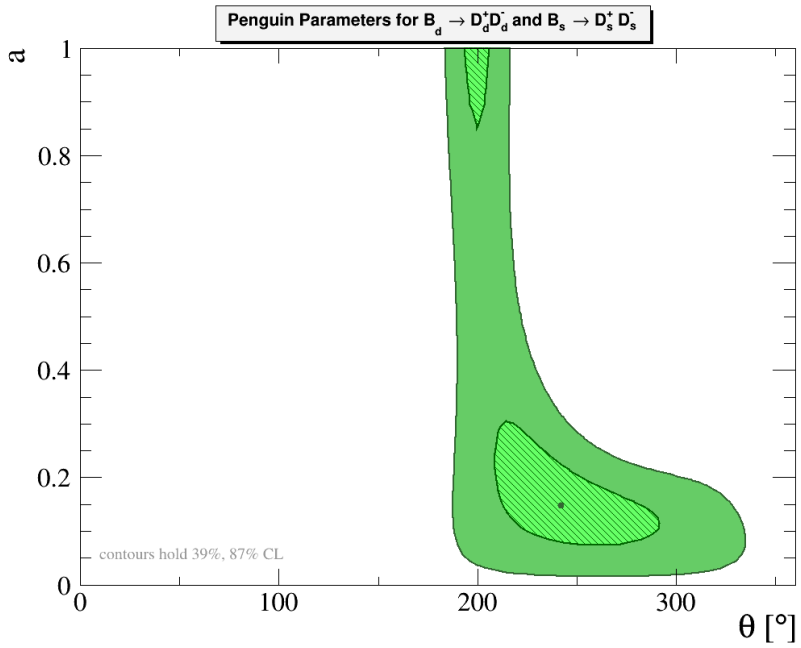

Figure 3.3: The fact that the shape of the contour has not changed means that the $B_s \to D_s^+ D_s^-$ decay does not provide any information that we can use to better determine the penguin parameters.

$$A_{CP}^{Dir}(B_s \to D_s^+ D_s^-) = \frac{1 - |\lambda|^2}{1 + |\lambda|^2} \tag{3.9}$$

$$A_{CP}^{Mix}(B_s \to D_s^+ D_s^-) = \frac{2|\lambda| \sin\left(\phi_s^{eff}\right)}{1 + |\lambda|^2} \tag{3.10}$$

where the ϕ_s in the equation above is the measured effective weak angle. For the CP-observables, this results in

$$\begin{aligned} A_{CP}^{Dir}(B_s \to D_s^+ D_s^-) &= 0.094 \pm 0.20\ (\text{stat}) \pm 0.02\ (\text{syst}) \\ A_{CP}^{Mix}(B_s \to D_s^+ D_s^-) &= 0.020 \pm 0.17\ (\text{stat}) \pm 0.02\ (\text{syst}) \end{aligned} \tag{3.11}$$

In theory it would be possible to determine the penguin parameters for the $B_s \to D_s^+ D_s^-$ decay as well, but the practical issue with that is the extra term of ϵ in Equation 2.46. This term epsilon reduces the contribution of the penguin diagrams with a factor ≈ 20. By imposing the U-spin symmetry, which interchanges the d and s quarks, one can argue that the penguin parameters themselves for the $B_s \to D_s^+ D_s^-$ should not be very different from those for the $B_d \to D_d^+ D_d^-$ decay. Mathematically, this comes down to $ae^{i\theta} = \epsilon a' e^{i\theta'}$. When GammaCombo is fed only the CP-observables from the $B_s \to D_s^+ D_s^-$ decay and it is instructed to fit for the penguin parameters, the result is a contour that spans the entire domain of θ and the physically acceptable domain of a. If we combine the data from $B_d \to D_d^+ D_d^-$ and $B_s \to D_s^+ D_s^-$, we see that the best fit contour has not changed with respect to Figure 3.2 where only $B_d \to D_d^+ D_d^-$ was involved.

Although the figure depicting the best fit for the penguin parameters will not give any new information because of this assumption, it is possible to extract the phase shift $\Delta\phi_s$ in this method and to determine the corrected angle ϕ_s^{corr}. Note that this ϕ_s^{corr} is different from the ϕ_s^{eff} that was taken from the LHCb measurement. In fact, ϕ_s^{corr} should coincide with the theoretical value resulting form Standard Model computations. Correspondingly, this means that we assume $\phi_s^{eff} = \phi_s^{corr} + \Delta\phi_s$. The word assumption is used, because it is also possible that there is an additional extra term $\Delta\phi_s^{NP}$. The possible New Physics contribution will not be considered at this time.
From this data, the phase shift due to the penguin diagrams is computed to be

$$\Delta\phi_s = (-0.007 \pm 0.011)\,\text{rad} = (-0.4 \pm 0.6)^\circ \tag{3.12}$$

It is interesting to see what the correlation between the penguin parameters a and ϕ_s are, as this will help in answering the research questions of this thesis. To determine the dependency of the magnitude on the penguin contributions to the decay process, Figure 3.4 is useful. It can be seen that the contour extends up to the $a > 1$ range, which physically is not relevant. Theoretically, there should actually be another χ^2 minimum in that range, but as discussed that will not be considered.

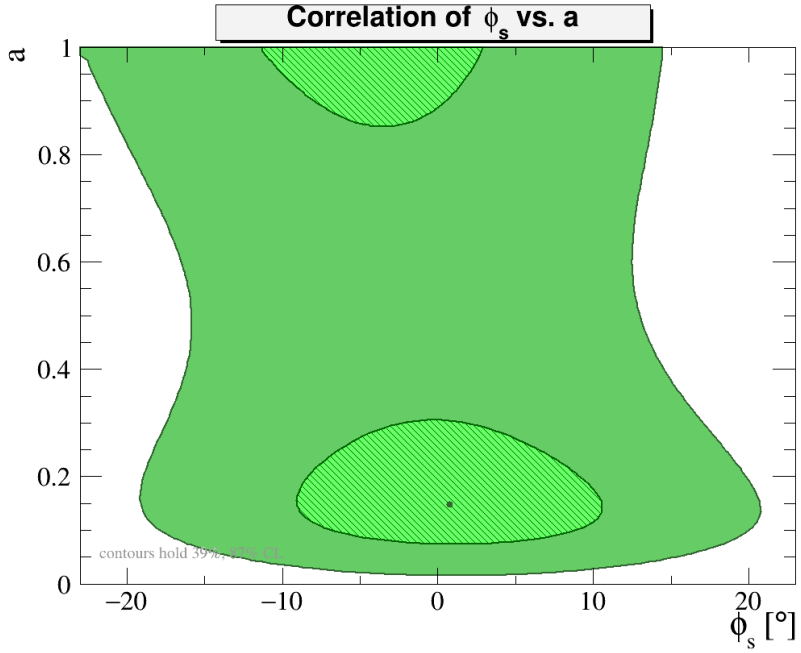

Figure 3.4: The correlation of the penguin parameter a with the weak angle ϕ_s.

The corrected value for ϕ_s would then be

$$\phi_s^{corr} = (0.02 \pm 0.17)\,\text{rad} = (1 \pm 10)^\circ \tag{3.13}$$

Below a summary is given of all numerics that have been obtained throughout this data analysis.

$$\begin{aligned} a &= 0.147 \pm 0.096 \qquad \text{and} \qquad \theta = (242 \pm 44)^\circ \\ \phi_s^{corr} &= (1 \pm 10)^\circ \qquad \text{and} \qquad \Delta\phi_s = (-0.4 \pm 0.6)^\circ \end{aligned} \tag{3.14}$$

For the sake of completeness, the obtained results are also stated in radians.

$$\begin{aligned} a &= 0.147 \pm 0.096 \qquad \text{and} \qquad \theta = (4.22 \pm 0.76)\,\text{rad} \\ \phi_s^{corr} &= (0.02 \pm 0.17)\,\text{rad} \qquad \text{and} \qquad \Delta\phi_s = (-0.007 \pm 0.011)\,\text{rad} \end{aligned} \tag{3.15}$$

Chapter 4

Discussion

In this chapter the results produced in the previous sections will be analysed to connect them with the underlying physics and make a bridge towards similar conclusions put forward on the literature. Besides drawing conclusions from these results, it is of course also important to assess the reliability of both the conclusion and the data. For this analysis it is important to reconsider the assumptions that were made to come to the current conclusions and assess the impact it may have in case the assumptions do not hold exactly.

4.1 Analysis of Assumptions

4.1.1 $SU(3)$-Symmetry

There are a number of assumptions made in this thesis to be able to obtain these results. This is useful, because if different decay topologies are related to each other, one can learn more about the system as a whole.
A large part of the conclusions in this work are based on the assumption of $SU(3)$- or U-spin symmetry. Theoretically it is known that this is a proper symmetry in the massless quark limit. Because the quarks are not actually massless, the symmetry is broken and corrections to the symmetry have to be made. If the contributions from these correction to the symmetries turn out to be so severe that the parameters from $B_d \to D_d^+ D_d^-$ cannot be related to $B_s \to D_s^+ D_s^-$, it is not possible to determine $\Delta\phi_s$ with reasonable confidence. There are methods to see whether the U-spin symmetry is actually 'intact enough' for us to make this assumption; the analysis of ratios of branching fractions that was explained in the Theory section comes to mind. This method allows for constraining the systematic errors by this symmetry breaking.

4.1.2 Ignored Decay Topologies

Another assumption that is done is the assumption that the contributions from the Penguin Annihilation, Exchange and Annihilation diagram are negligible. These diagrams are expected to be next order corrections for the amplitudes, but it is possible to do a more thorough

investigation of whether this is true.
To investigate this it is possible to employ the method of comparing branching fraction ratios. Because not all $B \to DD$ decays have contributions from the same topologies, by imposing the $SU(3)$-symmetry it becomes possible to investigate the contribution of for example the Penguin Annihilation and Exchange diagram in the $B_s \to D_d^- D_d^+$. This decay has not dominant contributions from the Tree or Penguin topologies.

4.1.3 Improvements in the Theory

Finally, a point of future research could be to inspect what happens if we do not stop writing the terms in the Wolfenstein parametrisation of the CKM-matrix (Equation 2.28) at order $\mathcal{O}(\lambda^4)$, but at higher orders. Although an increased factor of λ means a decrease of the term by a factor of $1/0.22548$, it could be that these higher order terms change the contribution of the penguin diagrams, resulting in different values for a and θ, where this change propagates all the way to the final result for $\Delta\phi_s$. Articles have already been written about further expansions of the idea that Wolfenstein started in his original paper, up to $\mathcal{O}(\lambda^7)$. [43].
The contribution from higher orders of λ become more important the more precise the measurements become; analysing these contributions by the time that a factor 5 in precision increase is reached is hence more important than for a factor 2 increase. Looking into these contributions should particularly be done if the contributions from other decay topologies have been quantified.

4.1.4 Ways to Constrain Assumptions

In the previous paragraphs, the assumptions underlying the produced results and their limitations are discussed. Fortunately, the validity of these assumptions can be investigated. This can be done by comparing the same observables that exist for different decay families. This section does is not trying to be a complete analysis, but rather an introduction to an additional topic of investigation. The used approach is based on a similar strategy in [8] and [26].
In the previous sections it was discussed that the $SU(3)$-symmetry was a useful symmetry because it allows comparing the amplitudes of $B_d \to D_d^+ D_d^-$ to $B_s \to D_s^+ D_s^-$ by setting $a' e^{i\theta'} = a e^{i\theta}$ and $\mathcal{A}' = \mathcal{A}$. This was useful, because it allowed for the determination of $\Delta\phi_s$ from $B_s \to D_s^+ D_s^-$ decays. Had this not been done, then there would have been too many parameters to solve for given the two constraints (the CP-violation observables) that were available. In the $B_s \to D_s^+ D_s^-$ decay the contributions from the Penguin diagrams are reduced by a factor ϵ, which is approximately by a factor of twenty, which also reflects in the Equations 2.43 and 2.44 that relate the observables to the Penguin parameters and the weak angles. This symmetry of $SU(3)$ however only holds in the limit of massless quarks. Since the quarks are in fact not massless, the actual symmetry is hence broken. This means that corrections can be made based on the parameters violating the symmetries to achieve a better description of the system. How large these corrections are is, can be investigated.
To investigate the order of these corrective effects, it is possible to use the branching fraction

ratios of the decays. If the effects are considered to be small enough, the symmetry can still be used to determine $\Delta\phi_s$. These corrections can be calculated by making use of the factorisation scheme. When employing this method to calculate the Penguin parameters, the factorisable effects should cancel in Equation 2.37. The symmetry breaking corrections should hence only appear in the non-factorisable parts. A parameter where this is relevant, is in the case of $\mathcal{A}$ as defined in Equation 2.37. Here, there is no fraction where the factorisable parts cancel and the corrective terms can also enter through factorisation.
These symmetry breaking effects are present in all of the discussed topologies (Tree, Penguin, Penguin Annihilation, Exchange, Annihilation). The strong interactions between the quarks are enclosed in the parameters $\mathcal{A}$ or $\mathcal{A}'$ and a or a' in the amplitudes discussed in the previous chapters. These contributions in itself are difficult to compute from theory due to how the coupling constant of the strong force scales with different energies and can in fact not be factorised. By using the branching fraction ratios, which comes down to measuring the fraction of the decay rates of the decays, the idea is that the contribution from the symmetry breaking effects can be constrained.

The branching fraction ratios can also be written as a function of the penguin parameters $a^{(\prime)}$ and $\theta^{(\prime)}$. This relation is shown in Equation 4.1. This means that once these parameters have been determined through another analysis, it is possible to estimate the value for the branching fraction ratio.

$$H = \frac{1 - 2a\cos(\theta)\cos(\gamma) + a^2}{1 + 2\epsilon a'\cos(\theta')\cos(\gamma) + \epsilon^2 a'^2} = -\frac{1}{\epsilon}\frac{A_{CP}^{Dir}(B_d \to D_d^+ D_d^-)}{A_{CP}^{Dir}(B_s \to D_s^+ D_s^-)} \tag{4.1}$$

It is also possible to derive the branching fraction ratios from experimental results. The experimental results can be related to the the Penguin parameters by combining Equation 4.1 and 4.2. Knowing the Penguin parameters from other analyses and the branching fraction ratios, this gives enough constraints to be able to determine the fraction of $|\mathcal{A}'/\mathcal{A}|$.

$$H \equiv \frac{1}{\epsilon}\left|\frac{\mathcal{A}'}{\mathcal{A}}\right|^2 \frac{\mathrm{PhSp}(B_d \to D_d^+ D_d^-)}{\mathrm{PhSp}(B_s \to D_s^+ D_s^-)}\frac{\tau_{B_d}}{\tau_{B_s}}\frac{\mathcal{B}(B_s \to D_s^+ D_s^-)_{theo}}{\mathcal{B}(B_d \to D_d^+ D_d^-)_{theo}} \tag{4.2}$$

The other terms introduced in Equation 4.2 are not very involved; τ_{B_q} depicts the lifetime of the respective particle and $\mathrm{PhSp}(B \to DD)$ the available phase space volume for that transition. Remembering from elementary quantum mechanics that the probability for a transition between an initial- and final state is proportional to the volume in the phase space that the final state can reach. It is not unexpected that a similar expression shows up here. The derivation for the expression of the two-body phase space function can be found in [44], but the result is stated below in Equation 4.3.

$$\Phi(x, y) = \sqrt{(1 - (x + y)^2)\,(1 - (x - y)^2)} \tag{4.3}$$

Finally, the subscript *theo* in the branching fractions $\mathcal{B}$ is different from the experimentally observed branching fractions. This is due to the fact that branching fractions in practice are always measured as time integrated quantities, as a fraction from the total event yield. The theoretical values are computed in the flavour-eigenstates, ignoring the neutral meson oscillation by evaluating the branching fractions at $t = 0$. These oscillations do have an effect in the experimental value [45]. It is illustrative to see the equations for these quantities side by side,

$$\mathcal{B}(B_s \to f)_{theo} \equiv \frac{\tau_{B_s}}{2} < \Gamma(B_s^0(t) \to f) > \Big|_{t=0} \tag{4.4}$$

$$\mathcal{B}(B_s \to f)_{exp} \equiv \frac{1}{2}\int_0^\infty < \Gamma(B_s^0(t) \to f) > dt \tag{4.5}$$

In both equations the f represents the final state.

The branching fraction ratios have a second use: they can be used to make estimates about the contributions of the Feynman diagrams that were chosen to be ignored. This can be done in a similar way as for the branching fraction ratios above. Writing the amplitudes for different $B \to DD$ decays as fractions of the contributing topologies, it is possible to constrain the relative contributions [26].

An example of such an expression is given in Equation 4.8. In this branching fraction ratio the decays of $B_s \to D_s^+ D_s^-$ and $B_d^0 \to D_d^- D_s^+$ is studied. The branching fraction ratios are useful quantities to study, as they can be obtained from the same data as the data that is used for analysis of the Penguin diagrams; only the number of decays from multiple processes is required. The branching fraction of a decay, such as $\mathcal{B}(B_d^0 \to D_d^- D_s^+) = (2.11 \pm 0.18) \pm 10^{-4}$, are relative branching fractions, with respect to the total decay width. The sum of all branching fractions should hence sum to unity. The relative decay rate of this transition can also be related to this quantity; by multiplying the branching fraction by the total decay rate $\sum_f \Gamma(B_d \to f)$ with f all eligible final states, the decay rate of this transition is obtained.

As the branching fractions are closely related to the amplitude of a transition, by computing the ratio of the branching fractions it is also possible to obtain the ratio of amplitudes. The amplitudes can then again be expressed in terms of the hadronic parameters $\mathcal{A}$ and the contributions from the distinct topologies through b and ρ for every decay, similarly as was done for a and θ in Equation 2.37.

To illustrate the possibilities of the branching fraction ratios, the decays $B_d^0 \to D_d^- D_s^+$ and $B_s^0 \to D_d^+ D_d^-$ will be analysed in addition to the $B_d \to D_d^+ D_d^-$ and $B_s \to D_s^+ D_s^-$ decays used so far. Just as that the substitutions $b \to -\epsilon a'$ and $\rho = \theta'$ are made in Equation 2.40, the substitutions $b \to -\epsilon \tilde{a'}$ and $\rho = \tilde{\theta'}$ for the $B_d^0 \to D_d^- D_s^+$ decay is employed in Equation 4.8. In general, the parameters with both a tilde and a prime represent the parameters for the last mentioned decay. It is possible to do some reparametrisation on Equation 4.8. Just as the penguin parameters for the $B_d \to D_d^+ D_d^-$ and $B_s \to D_s^+ D_s^-$ could represent the relative contribution of the penguin diagrams compared to the tree diagrams, it is also possible to do the same for the Exchange and the Penguin Annihilation diagram.

$$\tilde{x'} \equiv |\tilde{x'}|e^{i\tilde{\sigma'}} \equiv \frac{E' + PA^{(c+t)\prime}}{\tilde{T'} + \tilde{P}^{(c+t)\prime}} \tag{4.6}$$

$$\varsigma' \equiv \frac{\hat{E'} + \hat{PA}^{(c+t)\prime}}{E' + PA^{(c+t)\prime}} \tag{4.7}$$

Remember that the hadronic parameter $\mathcal{A}$ contained information about the contribution of the topologies; it is possible to collect the fractional part of the Exchange and Penguin Annihilation diagrams in the parameter $\tilde{x'}$ for this branching fraction ratio, as the $B_d^0 \to D_d^- D_s^+$ has no contributions from the Exchange and Annihilation topology. $\tilde{\sigma'}$ is the strong phase difference between the terms.

$$\begin{aligned} \Xi(B_s^0 \to D_s^+ D_s^-, B_d^0 \to D_d^- D_s^+) &= \frac{A(B_s^0 \to D_s^0 D_s^+)}{A(B_d^0 \to D_d^- D_s^+)} = \left(\frac{A'}{\tilde{A'}}\right) \left[\frac{1 + \epsilon a' e^{i\theta'} e^{i\gamma}}{1 + \epsilon \tilde{a'} e^{i\prime\theta'}}\right] \\ &= \left[\frac{T' + P^{(c+t)\prime}}{\tilde{T'} + \tilde{P}^{(c+t)\prime}} + \tilde{x'} e^{i\tilde{\sigma'}}\right] \left[\frac{1 + \epsilon a' e^{i\theta'} e^{i\gamma}}{1 + \epsilon \tilde{a'} e^{i\theta'}}\right] \end{aligned} \tag{4.8}$$

Of course, this expression in itself is not very helpful. With only one equation (Equation 4.8), it is not possible to fit for two parameters such as $\tilde{x'}$ and $\tilde{\sigma'}$. When this ratio of branching fractions is combined with other branching fraction ratios, there can be enough information collected to solve for the relative contribution of the Exchange and Penguin Annihilation diagrams $\tilde{x'}$ strong phase difference. Not only other branching fraction ratios are quantities that can be used to help constrain the parameters that are under investigation, but the Penguin parameters for the corresponding decays can also be collected. These can be collected through the CP-asymmetries measured through the decays, just as was done in this thesis for the $B_d \to D_d^+ D_d^-$ decay.

An easy example of how to constrain these parameters can be given when the branching fraction ratio of $B_s^0 \to D_d^+ D_d^-$ and $B_d^0 \to D_d^- D_s^+$ is considered. This fraction is chosen in particular, because the description in terms of the contribution of the Exchange and Penguin Annihilation diagrams in $B_d^0 \to D_d^- D_s^+$ ($\tilde{x'}$) and the strong phase difference in $B_s^0 \to D_d^+ D_d^-$ (ς') results in a very simple expression: the expression in Equation 4.9The branching fraction for the last two decays can namely be written as [26]

$$\Xi(B_s^0 \to D_d^+ D_d^-, B_d^0 \to D_d^- D_s^+) = \left|\varsigma' \tilde{x'}\right| \tag{4.9}$$

The measurement for this ratio is taken from [46]. Looking at the parameterisation in 4.9 a hyperbolic shape is expected for the contour, with the asymptotes being the vertical and the horizontal axes

$$\Xi(B_s^0 \to D_d^- D_d^+, B_d^0 \to D_d^- D_s^+) = 0.25 \pm 0.031 \tag{4.10}$$

Looking at Figure 4.1, there indeed turns out to be a hyperbola. Drawing a well founded conclusion on the contribution of the exchange and penguin annihilation diagrams with respect to the tree and penguin diagram is not yet possible. The contribution of the exchange and penguin annihilation diagram is strongly correlated with the same diagrams, but for the

$B_s^0 \to D_d^- D_d^+$ decay.

there is enough data available to fit a contour in the $(\tilde{x}', \varsigma')$-plane. The respective contour is shown in Figure 4.1.

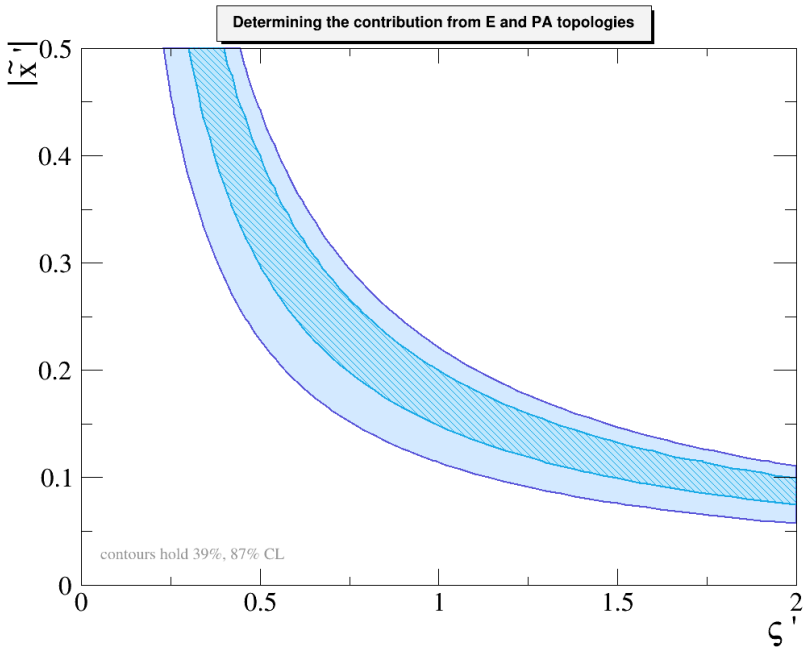

Figure 4.1: Contour of $\tilde{x}'$, which represents the relative contribution of the exchange- and penguin annihilation diagram to the tree and penguin diagram from the $B_s \to D_s^+ D_s^-$ decay.

Although at the current state no conclusion can be drawn, the main point of this section was to show that it is possible to determine the contributions of individual topologies. Had there been more time allotted for this project, this would have been an interesting area to continue in, as it helps determining the shift $\Delta\phi_s$ due to other topologies besides the Penguin diagrams. It is however a more involved process than just plotting several contours in the same figure; every ratio of branching fractions gives us a new parameter that can be solved for. The different decays in the $B \to DD$ family also all have different topologies through which their decays happen, which also complicates the matter. In the paper of Bel et al. [26] a collection of related decays is tabulated. There are eight different decays, which means that even more branching fraction ratios can be constructed to determine the symmetry correction. Not all fractions are equally useful, but it illustrates the richness of measurements available to investigate the system in more detail.

4.2 Analysis of Results

In the previous chapter the phase shift in the angle ϕ_s due to the correction of the penguin diagrams was assessed. Based on the obtained results, the measurement of $\phi_s^{eff} = (1.0 \pm 9.7)°$ by the LHCb-collaboration [42] is expected to contain a phase shift of $\Delta\phi_s = (-0.4 \pm 0.6)°$. Combining these observations, it is possible to distil the corrected value $\phi_s^{corr} = (1 \pm 10)°$. This

corrected value for ϕ_s has been computed through the relation $\phi_s^{corr} = \phi_s^{eff} + \Delta\phi_s$. The reported Standard Model value for ϕ_s, which should be compared against ϕ_s^{corr}, is $\phi_s =$ resulting from the global fit of the Unitarity Triangle [24]. The current result is still consistent with the Standard Model value within 0.3σ. The correction due to the Penguin diagrams is so small that it does not actually contribute visibly to the measurement - the phase shift is small enough to get lost in the truncation of insignificant digits in the final result for ϕ_s^{corr}.

This is at the current precision of these measurements, though. It is possible to increase the precision of the observation by performing more measurements over the run times of the particle accelerator projects. Currently, the largest uncertainty is in the determination of ${\phi_s^{eff}}_{D_s^+D_s^-}$ [1]; the measurement has a standard deviation of 10°, where the phase shift has a standard deviation of 0.6°. When this is compared with the measurement of ${\phi_s^{eff}}_{J/\psi\phi}$ in the $B_s \to J/\psi K^+K^-$ decay, which is used in the analysis of the Penguin diagrams in the $B_s \to J/\psi\phi$ decay, it is clear that the measurement for $B_s \to D_s^+D_s^-$ is a lot less accurate. The measurement of ${\phi_s^{eff}}_{J/\psi\phi}$ reports a value of $(0.041 \pm 0.025)\,\text{rad} = (-2.34 \pm 1.40)°$. The uncertainty in the last measurement is smaller by a factor of seven, allowing for a more precise determination of ϕ_s^{corr}. The difference in precision is due to multiple factors; the integrated luminosity at the time of computation of ${\phi_s^{eff}}_{D_s^+D_s^-}$ is $3\,\text{fb}^{-1}$, where for ${\phi_s^{eff}}_{J/\psi\phi}$ it is $4.9\,\text{fb}^{-1}$. More overall observations are however not a reason for the uncertainty to be different by this factor. The additional observations are not evenly distributed between $B_s \to D_s^+D_s^-$ and $B_s \to J/\psi\phi$ decays. The B_s-meson will more often decay to the $J/\psi\phi$ than to two $_s$ mesons because of the larger mass difference, so more observations of the first can be made with respect to the latter. An additional factor that is at play is the fact that the ϕ-meson decays to two K-mesons in $(49.2 \pm 0.5)\,\%$ of the time [47]. These K-mesons can then be detected in order to measure ${\phi_s^{eff}}_{J/\psi\phi}$. The D_s-mesons themselves are not directly observed, but rather through indirect measurements. The selection modes for the D_s-mesons in [42] are combinations of $D_s^+ \to K^+K^-\pi^+$ and $D_s^+ \to K^+\pi^-\pi^+$ plus the decays for the charge conjugates of the D_s mesons. The relative contribution of the $D_s^+ \to K^+K^-$ decay is only $(5.06 \pm 0.15)\,\%$ [48] and that for $D_s^+ \to \pi^+\pi^-\pi^+$ is only $(1.11 \pm 0.04)\,\%$ [49]. From this we can conclude that it is a lot harder to collect statistically significant data for the $B_s \to D_s^+D_s^-$ decay.

The current state of affairs is visualised in Figure 4.2. This figure again illustrates why the determination of the Penguin shift in $B_s \to D_s^+D_s^-$ currently can not be considered as a self-supporting result, but rather as an additional measurement in a collection of results. When the precision of the measurement of ${\phi_s^{eff}}_{D_s^+D_s^-}$ is increased, this may change the state of affairs. A detailed analysis of what will happen when more results are collected is a research project in itself, so in the next chapter a crude projection will be made for the coming years based on some simple estimates.

[1] Because different measurements for ϕ_s^{eff} will be discussed, an additional subscript is added to clarify which measurement is referred to when there is the possibility for ambiguity.

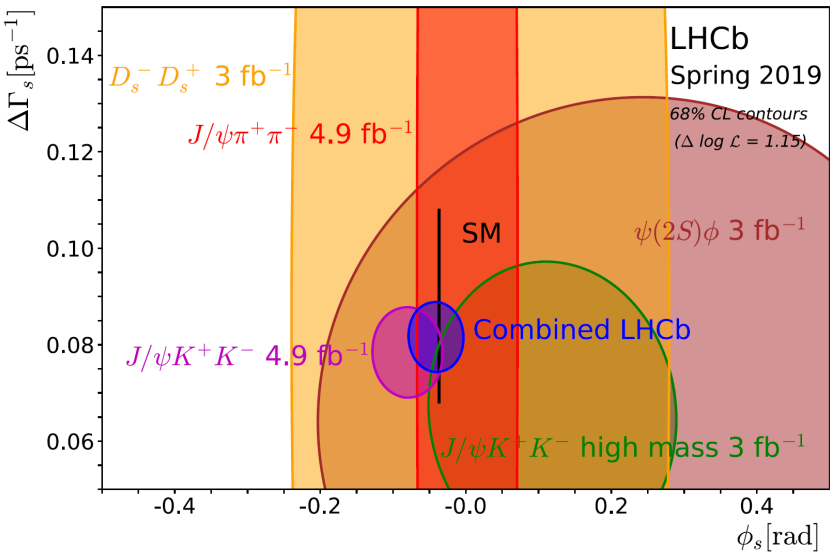

Figure 4.2: Regions of 68% confidence intervals in the $\phi_s - \Delta\Gamma_s$-plane for different LHCb measurements. The black bar denotes the predictions of ϕ_s and $\Delta\Gamma_s$ based on these results. It can be seen that the $D_s^- D_s^+$ measurement is one of the least significant measurements in the collection. Taken from: [50]

4.2.1 Comparing to the Literature

As the research here based on the previous section should not be considered by itself, it is important to consult the literature and see if the observations made here correspond with those in other research papers. Several aspects of this research can be compared with other publications. As was mentioned in the introduction, this research should be considered along the related research to the phase shift $\Delta\phi_s$ through the decays in the family of $B \to J/\psi X$. By comparing the results from these projects, it is possible to get a better idea of the effect of the Penguin diagrams than by studying them individually. If the same effect is observed in both projects, it strengthens the belief that this is due to the Penguin contributions. If the parametrisations for the $B_q \to D_q^- D_q^+$ and $B \to J/\psi X$ cause a deviation that pushes ϕ_s^{corr} in a different direction than that of the measurements analysed here of $B_q \to D_q^- D_q^+$, it is possible that there is some other mechanism at play that is contributing more.
In the analysis of Barel et al. [9] results of $\Delta\phi_s = 0.003^{+0.010}_{-0.012}\,\text{rad} = 0.14^{+0.54}_{-0.70}°$ and an effective mixing angle of $\phi_s^{eff} = -0.088^{+0.028}_{-0.027}\,\text{rad} = 5.0^{+1.6}_{-1.5}°$ rad were found. The numbers are not expected to be exactly the same, but it would build confidence in the results if the corrections due to the Penguin diagrams push the measurement of the respective ϕ_s^{eff} in the same direction. The current best estimate value of ϕ_s as computed from the Standard Model is $\phi_s = (-0.0376 \pm 0.0020)\,\text{rad} = (-2.15 \pm 0.11)°$ [9]. The correction of the Penguins thus pushes the measurement of the effective mixing angle more towards the current best estimate of ϕ_s, as seen in Figure 4.2. The measurement of the effective mixing angle is low when compared to theory computations and shifts upwards by the Penguin correction. When this is compared to the correction found in this research, $\Delta\phi_s = (-0.007 \pm 0.011)\,\text{rad} = (-0.4 \pm 0.6)°$ combined with ${\phi_s^{eff}}_{D_s^+ D_s^-} = 0.02 \pm 0.17 \pm 0.02\,\text{rad} = 1.1 \pm 9.7 \pm 1.1°$, it is observed that the measurement

of the effective mixing angle is too high and the Penguin corrections shifts the measurement downwards, towards the theoretical estimate of ϕ_s.

In the previous paragraph it is seen that indeed the corrections due to the Penguin contributions, the measurements come closer to the theoretically predicted value of ϕ_s. At the current precision, the results are not very significant. Telling apart the contributions from the Penguin diagrams or from New Physics is not something that can be done at the present time. The development of the machinery used here is still advantageous, though. When more precise measurements become available, the uncertainties in the results are bound to decrease and the tension between the Standard Model value and the measured value of ϕ_s^{corr} could increase in favor of New Physics. Instead of only the Penguin correction being present, the contributions to the effective mixing angle could then be constructed as $\phi_s^{corr} = \phi_s^{eff} + \Delta\phi_s^{Pen} + \Delta\phi_s^{NP}$. For the $B_s \to D_s^+ D_s^-$ decay, this is currently only a desire for the future. For the $B^0 \to J/\psi X$ decay family, this has already been attempted [9].

It is not only possible to compare the results obtained in this research with another decay family. Another comparison that is possible is to compare the results of the Penguin parameters in the $B_d \to D_d^+ D_d^-$ decay to other publications. In Bel et al. [26], the following result was found for the penguin parameters in the $B_d \to D_d^+ D_d^-$ decay.

$$a = 0.35^{+0.17}_{-0.23} \qquad \theta = 216^{+23\circ}_{-29} \tag{4.11}$$

Which are to be compared with the results $a = 0.147 \pm 0.096$ and $\theta = (4.22 \pm 0.76)\,\text{rad} = (242 \pm 44)^\circ$. The analysis of Bel et al. was performed in 2015 and is slightly different from the analysis used here. In 2016, the LHCb collaboration produced an additional measurement of the CP-observables in the $B_d \to D_d^+ D_d^-$ decay that can be used along with the measurements of Belle and BaBar. Furthermore, the analysis of 2015 also used the H-observable that is based on the branching fractions of $B_d \to D_d^+ D_d^-$ and $B_s \to D_s^+ D_s^-$ (see also Equation 4.1). This observable is not theoretically clean, as it is susceptible to $SU(3)$ breaking corrections. The contribution of this observable to the determination of the Penguin parameters can be observed in Figure 4.3. Although the usage of the H-observable is not preferred, this figures shows that with more constraints, the solutions for large a can be excluded.

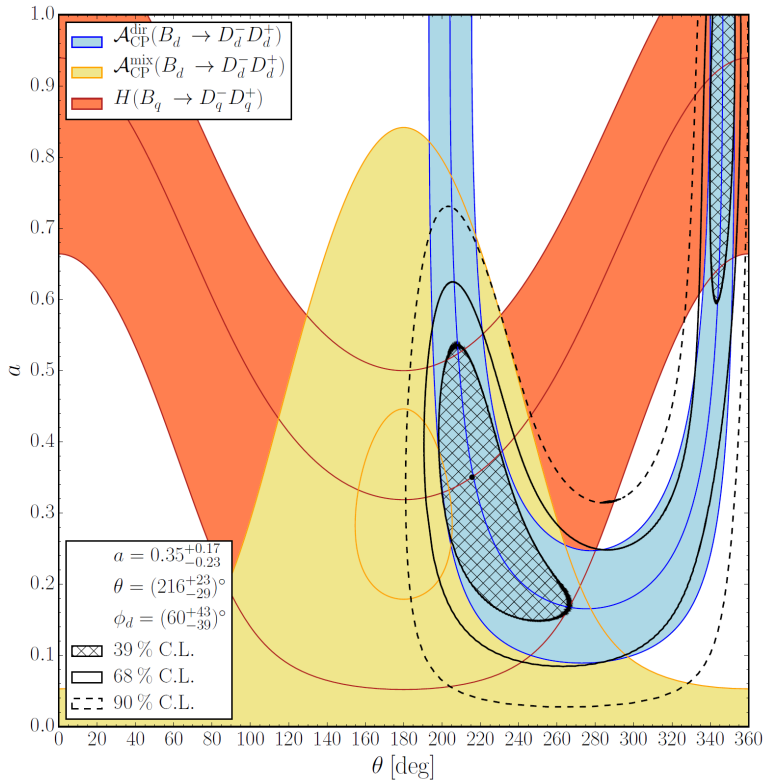

Figure 4.3: Illustration of the determination of the penguin parameters a and θ from Bel et al. Taken from: [26]

Chapter 5

Future Prospects

As discussed in the first two chapters of this thesis, it is possible to make a crude estimate of what will happen with the precision of the results produced due to new measurements becoming available. That this is a reasonable thing to do can be argued by considering the current developments in particle accelerations that produce measurements that can be used in this analysis.

5.1 Arguments for Increased Precision

From the obtained results in the previous chapters, no definitive conclusions can be drawn. The results produced in this thesis do not give evidence for the requirement of the Penguin shift in the measurements of ϕ_s. From this logically follows that constraining the contribution of New Physics at the boundaries of the Standard Model is a bridge too far. It is reasonable to assume that in the future the precision of measurements will increase because of several reasons. Firstly, as data collection continues, the number of events that are available for inspection necessarily increases. This comes together with bigger precision. Besides the experiments running longer, there are other factors that increase the precision of the measurements.
Most of the CP-observables cited in this thesis are the result of one of three institutes: Belle, BaBar or LHCb. The BaBar experiment, located at Stanford, has ceased data acquisition in 2008 [51].
The Belle experiment on the other hand has received an update that was finalised in 2018 and has been collecting data since finalising that project. The upgrades that were done to get to the current state of affairs for Belle II were done to the detection instruments themselves and to the readout electronics. Among the upgrades were new scintillation detectors that have been added in the forward direction, two Cherenkov detectors that have been added, and the replacement of the inner layers of the vertex detectors by have been replaced by different field effect transistors. With these upgrades in mind, the target dataset for Belle II has been set to $50\,\mathrm{ab}^{-1}$, as compared to the $988\,\mathrm{fb}^{-1}$ for Belle [7].
An update is scheduled for the LHCb detector in the coming years as well [6]. During the upgrade process, changes will be made to the detectors and the readout process. For one, the hardware-based trigger step $L0$ will be removed. The proton-proton collisions at the detector

occur at a frequency of 40 MHz where $L0$ reduced the event rate to 1 MHz. Originally this was because at the time of construction, a higher read-out rate could not be handled by the subdetectors. After the development of the past years, it is possible to handle such an amount of data and $L0$ can be removed. The components in the readout scheme will then have access to higher readout rates. The high-level trigger (HLT) will perform full reconstruction of events at a rate of 30 MHz as opposed to 1 MHz, allowing for a full reconstruction of events at a rate of $20 - 100$ kHz. It is not the case that the factor 40 increase in initial observations generates a factor of 40 more data that can be analysed, but it allows for a better selection of which events to keep and which to discard. With the modified Vertex Locator (VELO) which will move closer to the beam (8.4 mm to 5.1 mm) and less detector material between the vertex and the tracking layers, it is possible to make better measurements of the impact parameter. The Ring Imaging Cherenkov (RICH) detectors which will feature optimized mirrors and an increased readout rate. Another major addition are the Scintillating Fiber (SciFi) detectors. The estimate is that the LHCb-detector collect $50\,\text{fb}^{-1}$ of data by the end of run 4 due to these and other improvements. The work on this upgrade started after the completion of run 2, during which an integrated luminosity of approximately $8\,\text{fb}^{-1}$ was reached.
All these efforts will increase the amount of data that is available, which in turn will decrease the uncertainty that are intrinsic to the measurements. Because the upgrades described earlier do not give exact numbers on the increase of precision that is to be expected, several future prospects have been drafted up. The process of generating these prospects is straightforward. All currently available measurements have been averaged according to their statistical weights - the inverse square of their uncertainties - and the corresponding error has been propagated. The uncertainty of the measurement has then been reduced by a factor of two, as an estimate of the integrated luminosity obtained over the next five years, and a factor of five as an estimate of the integrated luminosity of the relevant collaborations around 2040.
The fundamental probability distribution that lies behind this process is a Poissonian probability distribution, as the CP-observables are based on a process of counting particles. The Poissonian probability distribution is given as $\mathcal{P}(k,\lambda) = \frac{\lambda^k e^{-\lambda}}{k!}$, but more importantly, the standard deviation is $\lambda^{1/2}$, which means that the standard error in the mean is $\sigma_m = \sqrt{\lambda/N}$. Since the integrated luminosity increases by a factor of 6.25 that would mean that σ_m decreases by a factor of ≈ 2.5 at the end of run 4. As this estimate is only based on the increased integrated luminosity while the detection efficiency will also increase, a factor 2 indeed seems like a safe estimate.

5.2 Projection of Possible Future Results

With the estimates made in the previous chapter, it does not seem unreasonable to decrease the uncertainties in the averages of the measurements by a factor of 2 or 5.

To visualise how big these improvements in accuracy will be, Figure 3.3 is drawn here again in Figure 5.1, but with three different contours. Each of the contours represents a possible scenario: no change, which is 'Current Precision', a $\times 2$ improvement, or a $\times 5$ improvement.

Observable	Current σ	$\times 2$ improvement	$\times 5$ improvement
a	0.096	0.049	0.021
θ	0.76 rad=44°	0.39 rad=22°	0.17 rad=9.7°
$\Delta\phi_s$	0.011 rad=0.6°	0.006 rad=0.3°	0.003 rad=0.2°
ϕ_s^{corr}	0.17 rad = 9.7°	0.085 rad = 4.9°	0.034 rad = 1.9°

Table 5.1: Future prospect of uncertainties in case of accuracy improvements.

The fit parameters for these future scenarios are given in Table 5.1. Of course, the best fit parameters do not change, as the central values itself are assumed not to change - only the uncertainties are reduced.

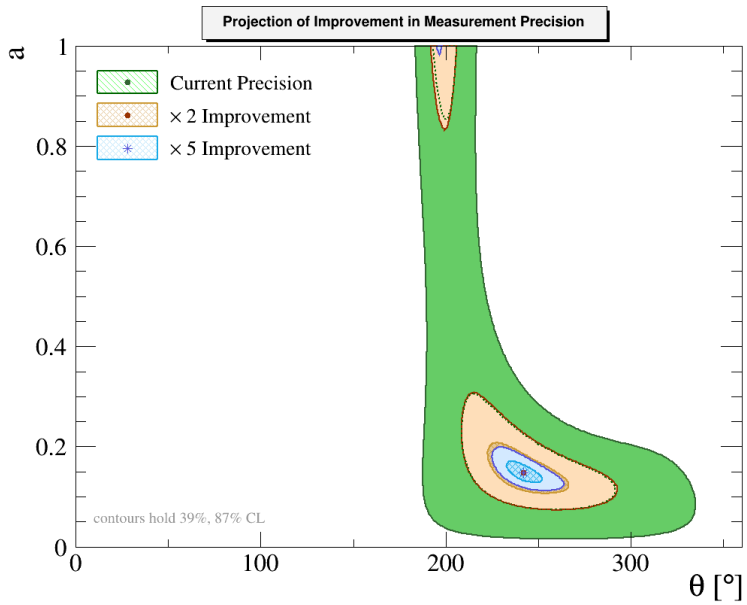

Figure 5.1: Three possible scenarios for the precision with which we might be able to determine the penguin parameters.

A figure showing the future projection for the correlation between a and ϕ_s is shown in Figure 5.2. In the results with current precision, the second solution for $a > 1$ is still connected to the best fit within the 39% Confidence Level contour. In the case of the "$\times 2$ Improvement", the two solutions are no longer connected within this Confidence Level. This is even more so the case for the "$\times 5$ Improvement". This second solution indicated by these contours will however still be excluded based on the argument that the solution is expected to be smaller than R_b, as discussed in previous sections.

The tension with the Standard Model is still not very significant - even at a precision increase with a factor five. Remember that the current theoretical estimate for $\phi_s = (-2.15 \pm 0.11)°$. This brings the tension between ϕ_s^{corr} and ϕ_s as computed from the Standard Model to 1.5 standard deviations, which is no significant evidence. The result of the $B_s \to D_s^+ D_s^-$ analysis in itself is therefore not going to bring conclusive evidence to the question of whether New Physics may exist on the boundaries of the Standard Model.

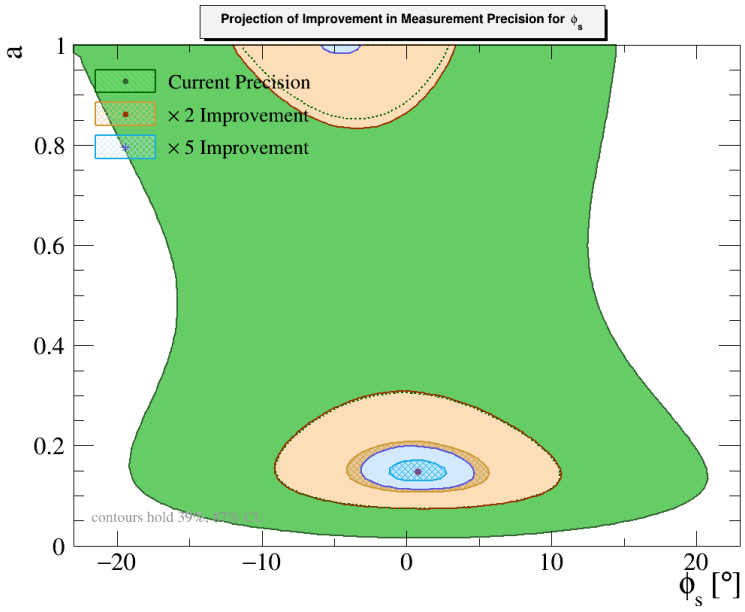

Figure 5.2: Three possible scenarios for the precision with which we might be able to determine the weak angle ϕ_s.

Of course, the analysis of future results also has to be considered in conjunction with the other available deacy channels that analyse ϕ_s and its constraints. Looking back at Figure 4.2, the measurements are scattered on both sides of the theoretical prediction of the Standard Model. This means that it is not only possible to compare the theory and the experimental values, but also the different experimental values amongst each other. In this thesis, the results seemed to converge towards each other. When this trend does not continue in the future, there may also be different mechanisms at play that are as of yet unknown. Another interesting situation would occur when the precisions for the measurements increase, while the central values don't change. This would result in the confidence-level contours in Figure 4.2 becoming smaller, to the point where perhaps there is no overlap with the theoretical value and the central values for different decay channels are not compatible anymore. If such a situation occurs, it opens up new areas for theoretical development and experimental investigations.

Chapter 6

Conclusion

The main objective of this project was the analysis of the penguin diagrams in the $B_d \to D_d^+ D_d^-$ and $B_s \to D_s^+ D_s^-$ decay and determining the shift $\Delta\phi_s$ that is introduced due to these diagrams. This phase shift is included in measurements of the angle ϕ_s^{eff}, but currently the entirety of ϕ_s^{eff} is ascribed to the leading order Tree diagrams. Constraining the phase shift $\Delta\phi_s$ is important, because possible New Physics may also introduce a phase shift $\Delta\phi_s^{NP}$ in the angle ϕ_s^{eff}. Without constraining the next order terms - in this case the Penguins diagrams - it is not possible to say something about these possible New Physics contributions.
To determine the phase shift $\Delta\phi_s$, the relation between CP-observables that originate from the decay of these B-mesons and the Penguin diagrams is investigated. Because it is possible to relate these observables to the Penguin parameters a and θ, it is also possible to relate these observables to $\Delta\phi_s$.
To model this relation, a module in the Gammacombo framework was programmed. This framework enables convolution of measurements relating to different parameters, through the underlying theoretical relations that are programmed in the module. The framework allowed for inputting measurements of the CP-observables A_{CP}^{Dir} and A_{CP}^{Mix}, such that these could be used in a fitting procedure (A log-likelihood minimization of the χ^2-function) for the penguin parameters a, θ and $\Delta\phi_s$.
It is not possible to directly determine reliably the shift $\Delta\phi_s$ from the Penguin contributions in $B_s \to D_s^+ D_s^-$ that are parametrised by the Penguin parameters a' and θ'. To solve this problem, the analogous decay $B_d \to D_d^+ D_d^-$ was considered. These two decays are similar and relate to each other through the U-spin symmetry. By determining the Penguin parameters that are affecting the CP-observables of the $B_d \to D_d^+ D_d^-$ decay and assuming the Penguin parameters are the same for $B_s \to D_s^+ D_s^-$, it is possible to determine $\Delta\phi_s$ using the CP-observables of the latter. Using the obtained phase shift $\Delta\phi_s$ it was possible to find a corrected value from the measurements of ϕ_s^{eff}. The corrected value ϕ_s^{corr} are still consistent with the Standard Model within a confidence limit of 0.3σ. The central value from the corrected phase differs from that of the Standard Model prediction, but at the current resolution it is not warranted to say that the values are irreconcilable. The Penguin diagrams shift the observed value ϕ_s^{eff} more towards the value predicted from the Standard Model, but at the current precision these corrections are only working in the margin of error. Would the uncertainties on these measurements be signif-

icantly smaller while the central value remained stable, there would have been more conclusive results regarding the Penguin shift and possibly even room for interpretation in the aspect of New Physics contributions. At current precision, this is however not the case.

The numerical results for the shift due to the Penguin diagrams and the final value for ϕ_s^{corr} are given below.

$$\Delta\phi_s = (-0.007 \pm 0.011)\,\text{rad} = (-0.4 \pm 0.6)^\circ \tag{6.1}$$

and the corrected weak angles

$$\phi_s^{corr} = (0.02 \pm 0.17)\,\text{rad} = (1 \pm 10)^\circ \tag{6.2}$$

At the current time, the uncertainties in these results are still quite large. The shift in ϕ_s deviates from zero with a strength of only 0.3σ. Although this does indeed not seem like a significant result like discussed in the previous paragraph, there is some consolation to be found in other research, where they obtained similar results. In [26] the shift from the Penguin diagrams pushed the measurement of ϕ_s^{eff} more towards the theoretical value of ϕ_s as predicted from Standard Model computations. Had the shift in the $B_s \to D_s^+ D_s^-$ and $B_s \to J/\psi X$ decays shifted the result not both towards that same predicted value, other dominating effects might be at play. As this is not the case, the corrections due to the Penguin diagrams indeed have to be taken into account if one has the ambitions to for example compute the New Physics contributions in this parameter.

The low statistical significance of the results in this research do however not imply that there will not be any significant results popping up in the near future. With the Belle II steadily collecting data and the work currently being performed on the LHCb detector [52] and the estimates on the improvements being made, careful estimates of the implications for these results are in place. Assumed that the central values for these parameters do not change, the shift in ϕ_s may be improved to a 0.7σ deviation in case of a factor two improvement, or a 1.5σ improvement in case of a factor five improvement. The biggest problem currently resides in the uncertainty of the measurement of ϕ_s^{eff}, which even after a $\times 5$ improvement is still expected to be 2.0°. If this is indeed where the results end up, the measurements of ϕ_s^{corr} would still not be viable evidence for New Physics.

Besides expanding the field by looking for New Physics, there are also improvements to be made in the basis for this project to reduce systematic errors. The broken $SU(3)$-symmetries introduce corrections to the results that are reported here. The other decay topologies, that were ignored in the analysis for this thesis, also bring corrections. These become more important as the precision of $\Delta\phi_s$ becomes higher. Finally, the theory can also be expanded to obtain more precise results. A higher order expansion of the Wolfenstein parametrisation is an example of this, but this is expected to have a smaller effect than preceding suggestions.

To get a completer view of the Standard Model, continuing the analysis of the Penguin diagrams is a useful tool. If one wants to look for evidence of New Physics or even correctly interpret current results, it is even required to incorporate the Penguin diagrams in the analy-

sis. Although the future of these results is no shining light based in a larger data set available for analysis alone, together with the reduction of systematic uncertainties it will be possible to increase the precision even further.

Acknowledgements

I would like to thank Kristof De Bruyn for guiding me through the process of writing this thesis. Where I ran into difficulties working on this project from home throughout the Corona pandemic, I can imagine that it is equally difficult for a supervisor to keep track of what his student is doing. His often immediate and extensive feedback to ideas, excerpts or presentations is greatly appreciated. I also learned a lot from his experience in communicating findings in these topics to people both in- and outside of this specific field.
I would also like to thank the LHCb Groningen group for sharing different views on topics we shared during our weekly meetings - even though not even remotely all topics were related to our running projects.

Bibliography

[1] N. Cabibbo and R. Gatto, *Consequences of Unitary Symmetry for Weak and Electromagnetic Transitions*, Il Nuovo Cimento (1955-1965) **21** (1961) 872.

[2] M. Kobayashi and T. Maskawa, *CP-Violation in the Renormalizahle Theory of Weak Interaction*, .

[3] *The Nobel Prize in Physics 2008*, https://www.nobelprize.org/prizes/physics/2008/summary/.

[4] J. H. Christenson, J. W. Cronin, V. L. Fitch, and R. Turlay, *Evidence for the* 2π *Decay of the* K_2^0 *Meson*, Physical Review Letters **13** (1964) 138.

[5] K. Izlar, *The March of the Penguin Diagrams*, https://www.symmetrymagazine.org/article/june-2013/the-march-of-the-penguin-diagrams, 2013. [Online; accessed 06-April-2021].

[6] L. collaboration *et al.*, *Physics case for an LHCb Upgrade II - Opportunities in flavour physics, and beyond, in the HL-LHC era*, 2019.

[7] K. James, *The Belle II Experiment*, CERN Proceedings (2017) 45 Pages.

[8] K. De Bruyn, *Searching for Penguin Footprints: Towards High Precision CP Violation Measurements in the B Meson Systems*, PhD thesis, Vrije Universiteit Amsterdam, 2015.

[9] M. Z. Barel, K. De Bruyn, R. Fleischer, and E. Malami, *In Pursuit of New Physics with* $B_d^0 \to J/\psi K^0$ *and* $B_s^0 \to J/\psi\phi$ *Decays at the High Precision Frontier*, arXiv:2010. 14423 [hep-ph] (2020) `arXiv:2010.14423`.

[10] A. Bettini, *Introduction to Elementary Particle Physics*, .

[11] M. E. Peskin and D. V. Schroeder, *An Introduction To Quantum Field Theory*, Avalon Publishing, 1995.

[12] A. Zee, *Quantum Field Theory in a Nutshell*, Princeton University Press, 2003.

[13] D. Lichtenberg, *Unitary Symmetry and Elementary Particles*, Elsevier, 1978.

[14] T. D. Lee and C. N. Yang, *Question of Parity Conservation in Weak Interactions*, Physical Review **104** (1956) 254.

[15] B. Kayser and D. London, *B-Decay CP Asymmetries, Discrete Ambiguities and New Physics*, Physical Review D **61** (2000) 116012, arXiv:hep-ph/9909560.

[16] LHCb Collaboration, R. Aaij *et al.*, *Observation of CP Violation in Charm Decays*, Physical Review Letters **122** (2019) 211803.

[17] Particle Data Group *et al.*, *Review of Particle Physics*, Progress of Theoretical and Experimental Physics **2020** (2020) , arXiv:https://academic.oup.com/ptep/article-pdf/2020/8/083C01/34673722/ptaa104.pdf.

[18] S. Descotes-Genon and P. Koppenburg, *The CKM Parameters*, Annual Review of Nuclear and Particle Science **67** (2017) 97, arXiv:1702.08834.

[19] L. Wolfenstein, *Parametrization of the Kobayashi-Maskawa Matrix*, Phys. Rev. Lett. ; (United States) **51:21** (1983) .

[20] J. Hardy and I. S. Towner, *V_{ud} from Nuclear Beta Decays*, in *Proceedings of 9th International Workshop on the CKM Unitarity Triangle — PoS(CKM2016)*, (Tata Institute for Fundamental Research (TIFR), Mumbai, India), 028, Sissa Medialab, 2017.

[21] The BaBar Collaboration, V. Lombardo, *Measurement of the CKM Angles Alpha and Gamma at the BaBar Experiment*, .

[22] LHCb, M. Kenzie, *Measurements of the CKM angle γ at LHCb*, PoS **BEAUTY2018** (2018) 004. 9 p.

[23] LHCb Collaboration, R. Aaij *et al.*, *Review of Particle Physics*, Physical Review D **98** (2018) 030001.

[24] J. Charles *et al.*, *Current Status of the Standard Model CKM Fit and Constraints on $\Delta F = 2$ New Physics*, Physical Review D **91** (2015) 073007, arXiv:1501.05013.

[25] M. Gronau, O. F. Hernandez, D. London, and J. L. Rosner, *Broken $SU(3)$ in Two-Body B Decays*, Physical Review D **52** (1995) 6356, arXiv:hep-ph/9504326.

[26] L. Bel *et al.*, *Anatomy of $B \to D\bar{D}$ Decays*, Journal of High Energy Physics **2015** (2015) 108, arXiv:1505.01361.

[27] S. Okubo, *φ-meson and unitary symmetry model*, Physics Letters **5** (1963) 165.

[28] K. Lingel, T. Skwarnicki, and J. G. Smith, *Penguin Decays of B Mesons*, Annual Review of Nuclear and Particle Science **48** (1998) 253, arXiv:hep-ex/9804015.

[29] R. Fleischer, *Theoretical Overview of CP Violation in B-Meson Decay*, arXiv:hep-ph/0006132 (2000) arXiv:hep-ph/0006132.

[30] R. Fleischer, *Flavour Physics and CP Violation: Expecting the LHC*, arXiv:0802. 2882 [hep-ph] (2008) arXiv:0802.2882.

[31] R. Fleischer, *CP Violation in the B System and Relations to $K \to \pi\nu\bar{\nu}$ Decays*, Physics Reports **370** (2002) 537, arXiv:hep-ph/0207108.

[32] S. Faller, R. Fleischer, and T. Mannel, *Precision Physics with $B_s^0 \to J/\psi\phi$ at the LHC: The Quest for New Physics*, Physical Review D **79** (2009) 014005, arXiv:0810.4248.

[33] Matthey William Kenzie, Till Moritz Karbach, Titus Mombächer, Maximilian Schlupp, Konstantin Schubert, *GammaCombo User Manual*, .

[34] ROOT Team, *ROOT: Analyzing Petabytes of Data, Scientifically.*, https://root.cern/.

[35] M. W. Kenzie *et al.*, *Gammacombo Manual*, 2019.

[36] E. Artin and M. Butler, *The Gamma Function*, Dover Books on Mathematics, Dover Publications, 2015.

[37] LHCb Collaboration, R. Aaij *et al.*, *Measurements of CP-Violation in $B^0 \to D^+D^-$ Decays*, Physical Review Letters **117** (2016) 261801, arXiv:1608.06620.

[38] The BaBar Collaboration, B. Aubert, *Measurements of Time-Dependent CP Asymmetries in $B^0 \to D^{(+*)}D^{(-*)}$ Decays*, Physical Review D **79** (2009) 032002, arXiv:0808.1866.

[39] The Belle Collaboration *et al.*, *Measurements of Branching Fractions and Time-Dependent CP Violating Asymmetries in $B^0 \to D^{*\pm}D^{\pm}$ Decays*, Physical Review D **85** (2012) 091106, arXiv:1203.6647.

[40] Belle, The Belle Collaboration and F. S. *Evidence for CP violation in B0 —> D+D- decays*, Phys. Rev. Lett. **98** (2007) 221802, arXiv:hep-ex/0702031.

[41] Heavy Flavor Averaging Group *et al.*, *Averages of b-Hadron, c-Hadron, and τ-Lepton Properties as of 2018*, arXiv:1909. 12524 [hep-ex] (2019) arXiv:1909.12524.

[42] LHCb Collaboration, R. Aaij *et al.*, *Measurement of the CP-Violating Phase ϕ_s in $B_s^0 \to D_s^0\bar{D}_s^0$ Decays*, Physical Review Letters **113** (2014) 211801, arXiv:1409.4619.

[43] Y. H. Ahn, H.-Y. Cheng, and S. Oh, *Wolfenstein Parameterization at Higher Order: Seeming Discrepancies and Their Resolution*, Physics Letters B **703** (2011) 571, arXiv:1106.0935.

[44] H. Murayama, *Notes on Phase Space*, http://hitoshi.berkeley.edu/233B/phasespace.pdf.

[45] K. De Bruyn *et al.*, *Branching ratio measurements of B_s decays*, Physical Review D **86** (2012) .

[46] LHCb Collaboration, R. Aaij *et al.*, *First observations of $B_s^- \to D^+D^-$, $D_s^+D^-$, and $D^0\overline{D^0}$ decays*, Physical Review D **87** (2013) .

[47] The BaBar Collaboration, J. P. Lees *et al.*, *Precision measurement of the $e^+e^-K^+K^-()$ cross section with the initial-state radiation method at BABAR*, Phys. Rev. D **88** (2013) 032013, arXiv:1306.3600.

[48] The Belle Collaboration, A. Zupanc *et al.*, *Measurements of branching fractions of leptonic and hadronic D_s^+ meson decays and extraction of the D_s^+ meson decay constant*, JHEP **09** (2013) 139, arXiv:1307.6240.

[49] CLEO, P. U. E. Onyisi *et al.*, *Improved Measurement of Absolute Hadronic Branching Fractions of the D_s^+ Meson*, Phys. Rev. D **88** (2013) 032009, arXiv:1306.5363.

[50] LHCb Collaboration, R. Aaij *et al.*, *Updated measurement of time-dependent CP-violating observables in $B_s^0 \to J/\psi K^+K^-$ decays*, The European Physical Journal C **79** (2019) 1.

[51] *The BaBar detector*, https://babar.heprc.uvic.ca/BFROOT/www/doc/workbook/detector/detector.html.

[52] A. Piucci, *The LHCb Upgrade*, Journal of Physics: Conference Series **878** (2017) 012012.